The Response of the *Limulus* Retina to Moving Stimuli: a Prediction by Fourier Synthesis

SCOTT E. BRODIE, BRUCE W. KNIGHT, and FLOYD RATLIFF

From the Rockefeller University, New York 10021

ABSTRACT The *Limulus* retina responds as a linear system to light stimuli which vary moderately about a mean level. The dynamics of such a system may conveniently be summarized by means of a spatiotemporal transfer function, which describes the response of the system to moving sinusoidal gratings. The response of the system to an arbitrary stimulus may then be calculated by adding together the system's responses to suitably weighted sinusoidal stimuli. We have measured such a spatiotemporal transfer function for the *Limulus* eye. We have then accurately predicted, in a parameter-free calculation, the eye's response to various stimulus patterns which move across it at several different velocities.

INTRODUCTION

The retina of the lateral eye of the horseshoe crab *Limulus polyphemus* has been the subject of extensive study (for reviews, see Hartline and Ratliff, 1972; Ratliff, 1974). In recent years, many of these studies have been addressed to the resolution of the eye's neural response into the actions of individual physiological subsystems at the cellular level. To this end, these studies have exploited techniques such as the optical isolation of single visual units and the electrical manipulation of single cells by means of intracellular microelectrodes. These methods are intended to suppress the broad integrative actions of the retina so that the actions of small components may be studied. The present study is complementary to this earlier work. Our goal is to develop a methodology which describes the neural action of the *Limulus* retina as an integrated whole. In principle, such a description should permit the quantitative prediction of the response of the retina to an arbitrary stimulus, as well as permit the further elucidation of the component cellular processes which underly the response.

In the present paper, we describe the application of such a methodology to the *Limulus* retina. We have developed a set of standard visual stimuli which generate responses which should completely characterize the retina. We also show how this characterization may be used to predict the response of the retina to light stimuli which vary both in space and in time. In the following paper (Brodie et al., 1978) we relate this description of the retina's integrative action to the underlying electrophysiological processes.

Our characterization task is greatly simplified by the fact that the *Limulus* retina is, to an excellent approximation, a "linear system;" that is, its response to

the sum of two stimuli is the sum of its responses to each stimulus presented separately (Knight et al., 1970). Although various nonlinear effects have been observed in the *Limulus* eye (Hartline and Ratliff, 1957; Barlow and Lange, 1974), they appear to be more prominent in the action of isolated visual units than in the response of the retina as a whole. Ultimately, the validity of our linear description should be judged by the extent of the agreement between the response of the eye and the predictions derived from the linear characterization.

THEORY

In this section we develop the theoretical basis for our analysis of the response of the *Limulus* retina. We begin with a very general discussion of linear systems analysis, and then specialize this treatment for application to the present measurements. We first make three fundamental assumptions about the system under study, which we may refer to as stationarity, linearity, and continuity.

By stationarity, we refer to the assumption that the properties of the system are stable with respect to time. In other words, we require that the system give the same response each time it is presented with the same stimulus. If we denote the stimulus as a function of time by $\mathcal{S}(t)$, and the corresponding response by $\mathcal{R}(t)$, and use an arrow ($\rightarrow$) to denote the action of the system under study, we may express the stationarity conditions as:

$$\mathcal{S}(t) \rightarrow \mathcal{R}(t) \text{ implies } \mathcal{S}(t-\tau) \rightarrow \mathcal{R}(t-\tau), \tag{1}$$

where τ is any constant shift in time. Of course, as nearly every biological system ages, and most neurophysiological preparations deteriorate, this assumption is necessarily an approximation.

Linearity refers to the assumption that the system obeys the superposition rule, that the response to a sum of inputs is the sum of the responses to the inputs taken separately. In symbols,

$$\mathcal{S}_1(t) \rightarrow \mathcal{R}_1(t),\ \mathcal{S}_2(t) \rightarrow \mathcal{R}_2(t) \text{ implies } \mathcal{S}_1(t) + \mathcal{S}_2(t) \rightarrow \mathcal{R}_1(t) + \mathcal{R}_2(t). \tag{2}$$

This is a very strong assumption, whose consequences will be vigorously exploited below. In general, many biological systems saturate when presented with very strong stimuli, but operate nearly linearly when presented with stimuli consisting of small fluctuations about a mean value.

The assumption of continuity states that small changes in the stimulus presented to the system produce only small changes in the response. This is a mild assumption for most systems in the middle of their operating range, but it often does not hold for systems at the extremes of their range. The effect of this assumption is to justify various mathematical manipulations below. For example, if x is some parameter and $\mathcal{S}_x(t)$ varies smoothly with x, then the continuity assumption allows us to assert the following continuous analog of Eq. 2:

$$\mathcal{S}_x(t) \rightarrow \mathcal{R}_x(t) \text{ implies } \int \mathcal{S}_x(t)\,dx \rightarrow \int \mathcal{R}_x(t)\,dx. \tag{3}$$

The assumptions of linearity and continuity together imply "weighted" versions of Eqs. 2 and 3:

$$\mathcal{S}_1(t) \to \mathcal{R}_1(t),\ \mathcal{S}_2(t) \to \mathcal{R}_2(t) \text{ implies } a\mathcal{S}_1(t) + b\mathcal{S}_2(t) \to a\mathcal{R}_1(t) + b\mathcal{R}_2(t); \quad (2')$$

$$\mathcal{S}_x(t) \to \mathcal{R}_x(t) \text{ implies } \int a(x)\mathcal{S}_x(t)\,dx \to \int a(x)\mathcal{R}_x(t)\,dx, \quad (3')$$

where a and b are numbers, and $a(x)$ is a function of x.

In general, a stationary, linear, continuous system (a "linear system," for short) can be completely characterized in several equivalent ways.

One such characterization consists of measuring the system's response to an "impulse," a stimulus of finite strength delivered within an arbitrarily short time. We will denote such a stimulus as a Dirac delta-function, $\delta(t)$. The response to such an impulse delivered at time $t = 0$ will be called the "impulse response," denoted $\mathcal{I}(t)$. The impulse response provides a complete characterization of a linear system by virtue of the following identity, which constitutes a fundamental property of the delta-function:

$$\mathcal{S}(t) = \int \mathcal{S}(u)\delta(t - u)\,du, \quad (4)$$

which expresses an arbitrary stimulus $\mathcal{S}(t)$ as a weighted combination of impulses occurring at different times; the weighting function is simply the stimulus function itself. The stationarity assumption implies that the response to the stimulus $\delta(t - u)$ is $\mathcal{I}(t - u)$; we may now apply Eq. 3′ to conclude

$$\mathcal{S}(t) \to \mathcal{R}(t) = \int \mathcal{S}(u)\cdot\mathcal{I}(t - u)\,du. \quad (5)$$

This is a formula for the response of the system to an arbitrary stimulus $\mathcal{S}$, given in terms of the impulse response $\mathcal{I}$.

An alternative characterization of a linear system can be obtained from Eq. 5 by considering the response of the system to a sinusoidal input. We may greatly simplify the calculations by adopting the complex-exponential notation for sinusoidal functions; we thus identify $\cos \omega t$ with the real part of the complex exponential $e^{i\omega t} = \cos \omega t + i \sin \omega t$. In general, any complex quantity is to be interpreted as representing its real part. This is valid, because "taking the real part" of a complex quantity obeys the superposition principle. With this convention, we choose for our stimulus $\mathcal{S}(t) = e^{i\omega t}$, a sinusoid of angular frequency ω. According to Eq. 5, for this stimulus, we obtain the response:

$$\begin{aligned} \mathcal{R}(t) &= \int e^{i\omega u}\mathcal{I}(t - u)\,du \\ &= \int e^{i\omega(t-u)}\mathcal{I}(u)\,du = \left(\int e^{-i\omega u}\mathcal{I}(u)\,du\right)\cdot e^{i\omega t}. \end{aligned} \quad (6)$$

Thus, the response of a linear system to a sinusoidal input $\mathcal{S}(t) = e^{i\omega t}$ is a sinusoid of the same frequency, multiplied by some (complex) number, which depends on the frequency, ω, and upon the impulse response, $\mathcal{I}$, of the system. We refer to this coefficient (considered as a function of ω) as the "transfer function" of the system, and denote it by $\mathcal{F}(\omega)$. We then have

$$\mathcal{R}(t) = \mathcal{F}(\omega)\cdot e^{i\omega t}, \quad (6')$$

where

$$\mathcal{F}(\omega) = \int e^{-i\omega t}\mathcal{I}(t)\,dt. \tag{7}$$

$\mathcal{F}(\omega)$ is the Fourier transform of the impulse response, $\mathcal{I}(t)$.

The transfer function $\mathcal{F}(\omega)$ provides a complete characterization of a linear system as a consequence of the following Fourier inversion formula:

$$\mathcal{S}(t) = \frac{1}{2\pi}\int e^{i\omega t}\tilde{\mathcal{F}}(\omega)\,d\omega, \tag{8}$$

where

$$\tilde{\mathcal{F}}(\omega) \equiv \int e^{-i\omega t}\mathcal{S}(t)\,dt. \tag{9}$$

This expresses an arbitrary stimulus $\mathcal{S}(t)$ as a weighted sum of sinusoids $e^{i\omega t}$; the weighting function $\mathcal{S}(\omega)$ is the Fourier transform of the stimulus. Applying Eqs. 3′ and 6′ to Eq. 8 yields

$$\mathcal{R}(t) = \frac{1}{2\pi}\int e^{i\omega t}\cdot\mathcal{F}(\omega)\cdot\tilde{\mathcal{S}}(\omega)\,d\omega. \tag{10}$$

This is an expression for the response of the system to an arbitrary stimulus $\mathcal{S}(t)$ in terms of the transfer function $\mathcal{F}(\omega)$. The response is the inverse Fourier transform of the product of the transfer function of the system and the Fourier transform $\tilde{\mathcal{S}}(\omega)$ of the arbitrary stimulus $\mathcal{S}(t)$.

It is appropriate to note here that although these two mathematical characterizations of a linear system are informationally equivalent, and each can be readily obtained from the other (by Eq. 7 and its Fourier inversion formula), the transfer function is often the more suitable characterization for direct laboratory measurement. This is because an impulse stimulus, though of finite total strength, has extremely large intensity (even in a laboratory realization of the theoretical infinite intensity). Such large signals may easily drive the system out of its linear range, or even damage it irreversibly (consider, for example, the study of a skin pressure receptor; in this case, an impulse takes the form of a sharp blow). Even when an impulse stimulus might not saturate the system, it may be difficult or impossible to provide a satisfactory impulse stimulus, especially if one studies a transduction whose only accessible input is the output of another transduction. In such a case, sinusoidal inputs are readily obtained, but impulses are unavailable.

We now proceed to formulate the analysis given above in terms appropriate to our particular experimental situation. We introduce coordinates on the *Limulus* lateral eye, with the x-axis horizontal, the y-axis vertical, and the origin centered on the test ommatidium (the ommatidium whose eccentric cell action potentials are being recorded). A completely general stimulus takes the form $\mathcal{S} = \mathcal{S}(x, y, t)$; for computational convenience, we restrict all further discussion to stimuli which depend only on x and t, that is, to stimuli which, at any time t, are constant along each vertical line. This reduces our problem to one dimension of time, and one of space. To further facilitate the analysis, we ignore the discrete structure of the *Limulus* eye, and assume instead that it is made of a continuum

of photosensitive elements, each possessing the same dynamical properties as the test ommatidium (Kirschfield and Reichardt, 1964). The ommatidia are sufficiently numerous and homogeneous so that this approximation is reasonably innocuous. Our final specialization is to restrict our calculations to predictions of the response to arbitrary intensity patterns which move uniformly across the eye. Although the Fourier methods outlined above are perfectly adequate to predict the response to an arbitrary time-varying stimulus, the restriction to stimuli of the form $\mathcal{S}(x, t) = \mathcal{S}(x - vt)$, where $\mathcal{S}(x)$ is some spatial pattern of illumination, and v is the drift velocity, greatly facilitates the calculation of the necessary Fourier transforms. Such stimuli, with $\mathcal{S}(x)$ arbitrary, and v at our disposal, are sufficiently general to provide a rigorous test of the adequacy of our characterization of the response of the eye.

This characterization is given in terms of a spatiotemporal transfer function, which generalizes the temporal transfer function of Eq. 7, above. We consider the response as a function of space and time, $\mathcal{R} = \mathcal{R}(x, t)$, and ask what is the response to a traveling spatial sinusoid $\mathcal{S}(x, t) = e^{i(\xi x+\omega t)}$. We may put this expression in the form $\mathcal{S}(x - vt)$ by writing

$$e^{i(\xi x+\omega t)} = e^{i\xi\left(x+\frac{\omega}{\xi}t\right)} = e^{i\xi(x-vt)},$$

where $v = -\frac{\omega}{\xi}$; this is the equation of a sinusoid of spatial frequency ξ moving with velocity $v = \omega/\xi$. In addition to our previous assumptions, we now assume that the response of the eye is invariant under translation (change of origin). This is the analogue for space of the stationarity assumption in time. With this assumption, an argument strictly analagous to that given above implies that the response $\mathcal{R}(x, t)$ to a sinusoidal input $\mathcal{S}(x, t) = e^{i(\xi x+\omega t)}$ is again a sinusoidal function of space and time, with the same spatial frequency ξ and the same temporal frequency ω. In other words, we have the input-output relation:

$$\mathcal{S}(x, t) = e^{i(\xi x+\omega t)} \quad \text{implies} \quad \mathcal{R}(x, t) = \mathcal{F}(\xi, \omega) \cdot e^{i(\xi x+\omega t)}, \tag{11}$$

where

$$\mathcal{F}(\xi, \omega) = \int\int e^{-i(\xi x+\omega t)} \mathcal{I}(x, t)\, dx\, dt \tag{12}$$

is a (complex) number depending on ξ and ω, given by the spatiotemporal Fourier transform of $\mathcal{I}(x, t)$, the response of the system to a spatiotemporal impulse (a vertical line at $x = 0$ flashed at the instant $t = 0$).

We now fit the pieces together to calculate the response of the system to an arbitrary moving pattern. We first obtain the Fourier transform of the spatial pattern of the stimulus $\mathcal{S}(x, t) = \mathcal{S}(x - vt)$:

$$\mathcal{S}(\xi) = \int e^{-i\xi x} \mathcal{S}(x)\, dx. \tag{13}$$

We also note the corresponding inversion formula:

$$\mathcal{S}(u) = \frac{1}{2\pi} \int e^{+i\xi u} \bar{\mathcal{S}}(\xi)\, d\xi. \tag{14}$$

Taking $u = x - vt$, we obtain a Fourier representation for the stimulus:

$$\mathcal{S}(x - vt) = \frac{1}{2\pi}\int e^{i(\xi x - \xi vt)}\tilde{\mathcal{S}}(\xi)\,d\xi = \frac{1}{2\pi}\int e^{i(\xi x + \omega t)}\tilde{\mathcal{S}}(\xi)\,d\xi, \tag{15}$$

where $\omega = \omega(\xi) = -\xi v$.
Applying Eq. 3′ to Eqs. 11 and 15 gives the final input-output relation:

$$\begin{aligned}\mathcal{S}(x - vt) \to \mathcal{R}(x, t) &= \frac{1}{2\pi}\int e^{i(\xi x + \omega t)}\cdot\mathcal{F}(\xi, \omega)\cdot\tilde{\mathcal{S}}(\xi)\,d\xi \\ &= \frac{1}{2\pi}\int e^{i(\xi x - \xi vt)}\mathcal{F}(\xi, -\xi v)\tilde{\mathcal{S}}(\xi)\,d\xi.\end{aligned} \tag{16}$$

Eqs. 11, 13, and 16 give a complete scheme for the characterization of our system: the transfer function $\mathcal{F}(\xi, \omega)$ may be obtained by measurement of the responses of the system to sinusoidal stimuli. Given $\mathcal{F}(\xi, \omega)$, the response to an arbitrary moving stimulus $\mathcal{S}(x - vt)$ may be obtained by taking the Fourier transform of the stimulus spatial pattern, multiplying by the transfer function, and taking the inverse Fourier transform. In this way, knowledge of the transfer function $\mathcal{F}(\xi, \omega)$ serves to completely characterize the system.

It is useful to assume that, in addition to being homogeneous (spatially invariant), the eye under study is isotropic, in the sense that the eye is indifferent to reflections about the test ommatidium ($x = 0$). Equivalently, the impulse response function shows the symmetry $\mathcal{J}(-x, t) = \mathcal{J}(x, t)$. This induces certain useful symmetries in $\mathcal{F}(\xi, \omega)$. For example, we have, from Eq. 12 that

$$\begin{aligned}\mathcal{F}(-\xi, \omega) &= \int\int e^{-i(-\xi x + \omega t)}\mathcal{J}(x, t)\,dx\,dt \\ &= \int\int e^{-i(\xi(-x) + \omega t)}\mathcal{J}(x, t)\,dx\,dt \\ &= \int\int e^{-i(\xi u + \omega t)}\mathcal{J}(-u, t)du\,dt \\ &= \int\int e^{-i(\xi u + \omega t)}\mathcal{J}(u, t)\,du\,dt = \bar{\mathcal{F}}(\xi, \omega).\end{aligned} \tag{17}$$

Now consider

$$\begin{aligned}\mathcal{F}(-\xi, -\omega) &= \int\int e^{-i(-\xi x - \omega t)}\mathcal{J}(x, t)\,dx\,dt \\ &= \int\int e^{-i(\xi x + \omega t)}\mathcal{J}(x, t)\,dx\,dt \\ &= \int\int e^{-i(\xi x + \omega t)}\mathcal{J}(x, t)\,dx\,dt \\ &= \bar{\mathcal{F}}(\xi, \omega),\end{aligned} \tag{18}$$

where the horizontal bars indicate complex conjugates, and where we have used the fact that $\mathcal{J}(x, t)$ is real.

Together Eqs. 17 and 18 imply

$$\mathcal{F}(\xi, -\omega) = \overline{\mathcal{F}(\xi, \omega)}. \tag{19}$$

The symmetry (Eq. 17) allows an important experimental simplification. We have:

$$e^{i(\xi x+\omega t)} \rightarrow \mathcal{F}(\xi, \omega)e^{i(\xi x+\omega t)}$$

$$e^{i(-\xi x+\omega t)} \rightarrow \mathcal{F}(-\xi, \omega)e^{i(-\xi x+\omega t)} = \mathcal{F}(\xi, \omega)e^{i(-\xi x+\omega t)}.$$

Adding, and dividing by 2, we obtain (using Eq. 2′)

$$\mathcal{S}(x, t) = e^{i\omega t}\cdot\cos \xi x \rightarrow \mathcal{F}(\xi, \omega)e^{i\omega t}\cos \xi x = \mathcal{R}(x, t). \tag{20}$$

Examining the output at $x = 0$ (the test ommatidium), we have

$$\mathcal{S}(x, t) = e^{i\omega t}\cos \xi x \rightarrow \mathcal{R}(t) \equiv \mathcal{R}(0, t) = \mathcal{F}(\xi, \omega)e^{i\omega t}. \tag{11′}$$

The implication of this equation is that we may determine the transfer function $\mathcal{F}(\xi, \omega)$ by examining the response of the eye to the stationary counterphase grating stimulus $e^{i\omega t}\cdot\cos \xi x$, instead of the drifting sinusoidal grating stimulus $e^{i(\xi x+\omega t)}$. The counterphase stimulus, which consists of a spatial sinusoidal grating, placed with a peak centered over the test ommatidium, modulated by multiplication by a time-varying sinusoidal signal, is especially well suited for experimental use (see below).

Again, by restricting our attention to the output at the test ommatidium, we obtain an analaogous version of Eq. 16:

$$\begin{aligned}\mathcal{S}(x, vt) \rightarrow \mathcal{R}(t) \equiv \mathcal{R}(0, t) &= \frac{1}{2\pi}\int e^{i\omega t}\mathcal{F}(\xi, \omega)\tilde{\mathcal{S}}(\xi)\,d\xi. \\ &= \frac{1}{2\pi}\int e^{-i\xi vt}\mathcal{F}(\xi, -\xi v)\tilde{\mathcal{S}}(\xi)\,d\xi.)\end{aligned} \tag{16′}$$

The assumption of linearity is also useful for reasons of experimental convenience. For example, it is unnecessary to present the stimuli of Eq. 11′ one at a time. Instead, we may form the linear combination stimulus

$$\mathcal{S}(x, t) = \sum_n c_n e^{i\omega_n t}\cos \xi x,$$

where the c_n are constants at our disposal and the ω_n are the temporal frequencies at which $\mathcal{F}(\xi, \omega)$ is sought. By Eq. 2′, we have, for this stimulus,

$$\mathcal{S}(x, t) = (\sum_n c_n e^{i\omega_n t})\cdot\cos \xi x \rightarrow \mathcal{R}(t) = \sum_n c_n\mathcal{F}(\xi, \omega_n)e^{i\omega_n t}. \tag{21}$$

For the fixed spatial frequency ξ, the transfer function can easily be recovered from this composite response with the aid of Fourier methods (see below). Indeed, the frequencies ω_n can be so chosen that all the second harmonics are distinct from the input frequencies. With such a choice of the ω_n, the (presumably negligible) response detected at second harmonic frequencies can be used as a simple monitor of the linearity of the system (Victor et al., 1977). Such a choice of test stimulus has two advantages in the present situation. First, it

substantially reduces the data acquisition time necessary to characterize the system response over the grid of spatiotemporal frequency points. Second, because such a stimulus contains modulation over a substantial range of temporal frequencies, it prevents the occurrence of "phase locking," a distinctly nonlinear phenomenon which affects many neural encoders driven predominantly at a single frequency (Knight, 1972 *a*). By choosing the weighting coefficients c_n roughly reciprocal to the anticipated magnitude $|\mathcal{F}(\xi, \omega_n)|$ of the transfer function at each frequency ω_n, one produces a response with roughly equal output power at each frequency ω_n. Under such circumstances, phase locking becomes exceedingly unlikely. Furthermore, this procedure optimizes the signal-to-noise ratio at each frequency.

In the preceding analysis, we have described the prediction of a response, $\mathcal{R}(t)$ from the knowledge of the stimulus $\mathcal{S}(x, t)$ and a spatiotemporal transfer function $\mathcal{F}(\xi, \omega)$, which may be determined by measuring the response to particular stimuli. For such analysis, the output function $\mathcal{R}(t)$ is in general a continuous function of time, and the input is is a continuous function of space and time. In our experimental situation, the input variable is straightforward. $\mathcal{S}(x, t)$ specifies the illumination incident on the eye at the position x, and time t. The output variable is more problematical. As described above, we limit our attention to the response of a single "test ommatidium," whose electrical activity is monitored as a train of discrete action potentials. In order to interpret this sequence of discrete events as a continuous function of time, we invoke a notion of "mean impulse density." To frame the definition of this output variable, we consider an ensemble of N statistically independent replicas of the test ommatidium, each presented with the same stimulus. Over any brief time interval $(t, t + \mathrm{d}t)$, we can determine the number, $m_N(t, t + \mathrm{d}t)$, of impulses occuring in the entire ensemble of N elements. As N increases, we expect to find at least a few impulses over even very short time intervals, at least in the absence of phase-locking. We define the mean impulse density $r(t)$ as a normalized limit of such impulse counts:

$$r(t)\,\mathrm{d}t \equiv \lim_{N\to\infty} \frac{1}{N}\, m_N(t, t + \mathrm{d}t). \tag{22}$$

Under our assumptions that the eye is dynamically homogeneous, the mean impulse density can be identified with the "population firing rate" (Knight, 1972 *a*).

In practice, only one specimen of the test ommatidium is available, precluding direct application of the definition (Eq. 22). We may assume however, that the responses of this single unit to successive presentations of the same stimulus are statistically independent, and replace the average in Eq. 22 with an average over repetitions of the same stimulus. Even in this case, however, direct calculation of $r(t)$ from the definition requires a great deal of data, and many procedures have been advocated for its optimization (see Appendix B). Fortunately, for our purposes, an explicit calculation of $r(t)$ is unnecessary; we need only its Fourier components at various frequencies. A least-squares method for estimating these parameters directly from the list of impulse occurrence times is discussed in Appendix B. With this method, we obtain our transfer function $\mathcal{F}(\xi, \omega)$ in terms of the transduction from light intensity to mean impulse density.

For the purpose of displaying the measured response to moving patterns, however, an explicit function of time is needed. Here, we have found an alternative output variable, the "mean instantaneous rate" to be convenient. We begin by defining, for any one sample of impulse train data, an "instantaneous rate" function $s(t)$. (This function, which

we define for all times t, generalizes the usual definition, which applies only to those times at which impulses occur.) At any time t, $s(t)$ is defined as the reciprocal of the duration of the interval between impulses in which the time t falls. We have

$$s(t) \equiv \sum_n \chi_{(t_n, t_{n+1})}(t) \cdot \frac{1}{t_{n+1} - t_n}, \tag{23}$$

where t_n is the time of occurrence of the n'th impulse, and

$$\chi_{(a,b)}(t) = \begin{cases} 1, & a < t \leq b \\ 0, & t \leq a \quad \text{or} \quad t > b \end{cases}.$$

Note that, for any time t, only one term in the summation in Eq. 23 is non-zero. Considering now M presentations of the identical stimulus, and denoting by $s_m(t)$ the instantaneous rate function observed in response to the m'th stimulus presentation, we define $\sigma(t)$, the mean instantaneous rate:

$$\sigma(t) \equiv \langle s_m(t) \rangle = \frac{1}{M} \sum_{m=1}^{M} s_m(t). \tag{24}$$

Thus, the mean instantaneous rate at any time t is the average, over all repetitions of the stimulus, of the reciprocals of the lengths of the intervals between impulses in which the time-point t happens to fall. If the overall impulse rate, ν, is very fast compared to the time scale of the response under study, the alternative output functions $r(t)$ and $\sigma(t)$ will be very similar; however, at low impulse rates or high modulation frequencies, the functions differ. One may nevertheless compare data given as $\sigma(t)$ with predictions derived from a transfer function obtained in terms of $r(t)$ by incorporating a transfer function which describes the transduction from one output variable to the other.

We now calculate such a transfer function, under the assumption that the modulation is sufficiently small that we may employ a perturbation analysis. It is convenient to break the overall transduction $r(t) \rightarrow \sigma(t)$ into two pieces: first, the transduction from mean impulse density to instantaneous rate, and then from instantaneous rate to mean instantaneous rate: $r(t) \rightarrow s(t) \rightarrow \sigma(t)$. The first transduction, from a population rate to a single unit rate, has been treated in great generality elsewhere (Knight, 1972 *a*); we simply cite the result: if each of an ensemble of identical neurons encodes a continuous signal into a sequence of impulses according to a "deterministic" law such that, for any given stimulus, t_{n+1} is a monotonic (steadily increasing) function of t_n, then the transduction from population rate to the instantaneous rate of a single unit corresponds to the transfer function

$$B(\omega, \nu) \equiv \frac{1 - e^{-i\omega/\nu}}{i\omega/\nu}. \tag{25}$$

To analyze the second transduction, from instantaneous rate to a mean instantaneous rate, we consider an encoder producing a sequence of impulses with sinusoidally modulated instantaneous rate. If such a device produces an impulse at time t, we have

$$s(t) = \nu + \epsilon e^{i\omega t}, \tag{26}$$

where ν is the mean rate, and $\epsilon << \nu$. If an impulse does not occur at the time t, $s(t)$ takes its value from the following impulse:

$$s(t) = \nu + \epsilon e^{i\omega t_{n+1}}, \qquad t_n < t \leq t_{n+1}. \tag{26'}$$

To obtain $\sigma(t)$, we average Eq. 26′ over all those times t_{n+1}, at which an impulse could immediately follow the time t. To first order, we have

$$\sigma(t) = \langle s(t) \rangle = \frac{1}{T}\int_t^{t+T} (\nu + \epsilon e^{i\omega t_{n+1}})\,\mathrm{d}t_{n+1}$$

$$= \nu + \frac{\epsilon}{T}\int_0^T e^{i\omega(t+\tau)}\,\mathrm{d}\tau \tag{27}$$

$$= \nu + \epsilon e^{i\omega t} \cdot \frac{1}{T}\int_0^T e^{i\omega\tau}\,\mathrm{d}\tau,$$

where $T \equiv 1/\nu$ is the mean interval between impulses. Subtracting the constant term ν and dividing by the input $e^{i\omega t}$ yields the transfer function from $s(t)$ to $\sigma(t)$:

$$\frac{1}{T}\int_0^T e^{i\omega\tau}\,\mathrm{d}\tau = \frac{e^{i\omega T} - 1}{i\omega T} = \frac{e^{i\omega/\nu} - 1}{i\omega/\nu} = \overline{B(\omega, \nu)},$$

namely the complex conjugate of $B(\omega, \nu)$, as defined in Eq. 25.

Now, if we start with a signal of the form $r(t) = Ae^{i\omega t}$, where A is any (complex) number, then the corresponding $s(t)$ signal will be given by $s(t) = A \cdot B(\omega, \nu)e^{i\omega t}$, and $\sigma(t) = A \cdot B(\omega, \nu) \cdot \overline{B(\omega, \nu)}e^{i\omega t} = A \cdot |B(\omega, \nu)|^2 e^{i\omega t}$. Taking A to be the spatiotemporal transfer function $\mathcal{F}(\xi, \omega)$ which relates stimulus $\mathcal{S}$ to the output variable r, we conclude

$$\begin{aligned} \mathcal{S}(x, t) = e^{i(\xi x + \omega t)} \rightarrow r(t) = \mathcal{F}(\xi, \omega)e^{i\omega t} \quad \text{implies} \\ \mathcal{S}(x, t) = e^{i(\xi x + \omega t)} \rightarrow \sigma(t) = |B(\omega, \nu)|^2 \mathcal{F}(\xi, \omega)e^{i\omega t}. \end{aligned} \tag{28}$$

Thus, if the transfer function in terms of $r(t)$ is $\mathcal{F}(\xi, \omega)$, then the transfer function in terms of $\sigma(t)$ is simply $|B(\omega, \nu)|^2 \cdot \mathcal{F}(\xi, \omega)$.[1]

For our *Limulus* data, the factor $|B(\omega, \nu)|^2$ has only a very slight effect on the results of the Fourier synthesis calculations. This is a consequence of the fact that our moving stimuli contained very little spectral power in the high frequency regime, where $|B(\omega, \nu)|^2$ differs significantly from unity. In other circumstances, this correction would have a more significant effect.

We note that this linear analysis applies, strictly speaking, only to the variations of the various functions about their mean level (light intensity, on input; and impulse rate, on output). This restriction is necessary, in part, because our experimental variables do not take on negative values. Furthermore, when considered as a function of absolute stimulus intensity, the response of most sensory transducers, including the *Limulus* eye, is decidedly nonlinear, and exhibits a nearly logarithmic response to time-independent stimuli which vary over many orders of magnitude (Stevens, 1975).

Finally, over periods comparable to our experimental trials, many transducers, including the *Limulus* eye, show considerable fatigue or adaptation, in violation of our assumption of stationarity. Such systems may be treated by linear methods only in terms of their fluctuations about a mean operating level which has been adjusted to include the effects of short-term adaptation. Thus, in the present study, to compare responses with linear predictions, the mean level and adaptation rate were measured, subtracted from the output signal,

[1] Our notation here recognizes the fact that in this paper we deal only with real ω; more generally, for complex ω, the transfer function is given by the analytic expression $B(\omega, \nu)B(-\omega, \nu)\mathcal{F}(\xi, \omega)$.

and then added back to the results of the linear calculation. We made no attempt to predict these mean output levels.[2]

MATERIALS AND METHODS

Stimulus

Patterns of light, varying in space and time, were formed on the screen of a large oscilloscope (Hewlett-Packard model 1321A High Speed Graphic Display, Hewlett-Packard Co., Palo Alto, Calif.) using analog voltages produced by a system of circuits designed for this purpose (Shapley and Rossetto, 1976), and digital-to-analog converters (DAC) controlled by a PDP 11/45 computer (Digital Equipment Corps., Maynard, Mass.). This time-varying pattern was then imaged by a high-quality camera lens (Nikon Nikkor f/1.2, focal length 55 mm, Nikon, Garden City, N. Y.) onto the flat surface of a fiber-optic taper, which was glued to the cornea of a *Limulus* eye. This fiber-optic device, supplied according to our specifications by Walter P. Siegmund of the American Optical Corp., Southbridge, Mass., conveyed the visual stimulus to the curved array of *Limulus* photoreceptors. The details of the optical system are discussed in Appendix A. The overall effect of this optical system was to convert a pattern 15 cm wide and 2 cm high on the oscilloscope face to a stimulus 1 cm wide and 0.13 cm high on the corneal surface. The height of the image, roughly one-fourth of the height of the eye, was chosen as a compromise between the theoretically desirable goal of illuminating the entire eye, and the need to illuminate a sufficiently narrow band to get an acceptably high impulse rate. (Larger stimuli produce low impulse rates by producing more lateral inhibition, and by spreading the same photon flux over a greater number of ommatidia).

For all stimuli produced, a high-frequency triangle-wave was applied to the Y-input of the display oscilloscope; the X-input was driven with a sawtooth waveform generated by the computer, and the Z-input (intensity) was driven by computer-generated signals synchronized to the X-input sawtooth. This arrangement produced a rectangle of light on the screen, whose intensity varied with horizontal position and time, but whose intensity was independent of vertical position. Three types of stimuli were used: a "setup" stimulus to align the stimulus coordinates with the test ommatidium; an "analysis" stimulus for measuring the spatiotemporal transfer function; and a "synthesis" stimulus which consisted of a uniformly drifting pattern of illumination.

The "setup" stimulus consisted of a single bright vertical line at $x = 0$ surrounded by a uniform dim background; this stimulus did not vary with time. This pattern was manually moved across the face of the oscilloscope until the bright line was centered on the test ommatidium, as indicated by monitoring its impulse-train discharge. This adjustment was generally reproducible to within $\pm$ 0.004 eyewidths,[3] and proved more than adequate for the purposes of these experiments.

[2] In the *Limulus* visual system, the use of signals consisting of perturbations about a mean level also allows us to ignore in the analysis the phenomenon of inhibitory thresholds (Hartline and Ratliff, 1957), a decidedly nonlinear effect. See also below.

[3] In our experimental apparatus, the width of the *Limulus* eye under study is the most natural unit for the horizontal coordinate. For a typical eye, this may be converted as follows: 1.0 eye widths = 1.0 cm = 40 ommatidial diameters (in the horizontal direction). The conversion to visual angle (in the horizontal direction) is somewhat complicated, because even though the ommatidia are rather evenly spaced, their optical axes diverge nonuniformly. Thus, in the center of the eye, an ommatidium subtends $\sim 6°$ of visual angle, but the whole eye (40 ommatidia in width) covers a total visual angle of only $\sim 200°$.

The "analysis" stimulus was produced by using for the Z-input of the display oscilloscope a signal which consisted of a constant offset plus the analog product of three computer-generated signals: a constant voltage (to control the total contrast); a "temporal modulation" signal whose value was changed before each sweep of the X-input sawtooth (each sweep lasted 0.01536 s; this yielded a temporal sampling rate of 65.1 Hz); and a "spatial modulation" signal, a rapid sinusoidal modulation synchronized to the X-input sawtooth so as to produce a cos ξx spatial pattern. (This is shown schematically as a block diagram in Fig. 1.) The X-sawtooth was obtained by rapidly producing 256 successive equally spaced voltage values with a DAC. This provided a spatial sampling mesh of 256 points/eye width (which corresponds to eight points per cycle at the highest spatial frequency used). The temporal modulation signal was a sum of eight sinusoids with

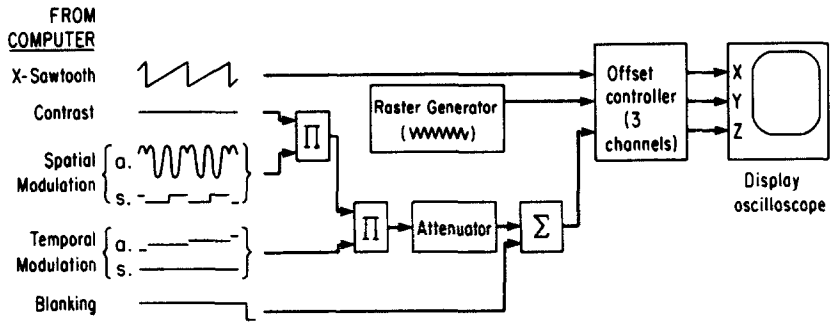

FIGURE 1. Block diagram of spatiotemporal stimulus generation. Π indicates analog multipliers; Σ indicates analog summer. The raster generator produces a free-running 100 KHz triangle wave for the Y-axis. The attenuator is a voltage divider set by hand to adjust overall contrast level. The offset controller adds analog signals to manually adjusted constant voltages. Three channels are provided: X and Y offset moves the stimulus origin on the oscilloscope face; Z offset adjusts mean illumination level. Two cycles of computer-generated input are shown at left (*a.* denotes analysis episodes; *s.* denotes synthesis episodes). Note spatial and temporal modulation are synchronized to X-sawtooth. Constant "contrast" voltage allows computer control of contrast level. "Blanking" signal darkens oscilloscope between experimental episodes.

frequencies 0.1, 0.233, 0.5, 1.033, 2.1, 4.233, 8.5, and 17.033 Hz.[4] The relative amplitudes of these components were 60, 50, 45, 30, 15, 10, 20, and 40, respectively.

The "systhesis" stimulus was generated in a similar manner, by holding the "temporal modulation" signal constant, and by producing the spatial modulation by sending to the DAC successive numbers from a list of intensities which described the arbitrary spatial pattern, synchronized to the X-sawtooth. By progressively shifting the phase of the intensity list with respect to the sawtooth, the pattern was made to drift across the screen at any desired rate.

By reversal of the order in which the X-sawtooth voltages were read out by the DAC, it was possible to reflect the synthesis stimulus about the test ommatidium, in order to verify our assumptions concerning the symmetry of the eye, and also to check the accuracy of the alignment of the stimulus origin with the test ommatidium. For the

[4] $(2^{n+1} - 1)/30$, in Hz.

synthesis stimuli, spatial resolution was upgraded to 512 points/eye width, at the expense of lowering the sweep rate to 39.1 Hz. (For comparison, the comparable temporal resolution for commercial television is 30 Hz in the U.S., 25 Hz in Europe; movies are typically shown at a frame rate of 24 Hz.) Spatial patterns were fixed at 2.0 eye widths in length, and were presented in a periodic fashion through a "window" one eye width wide, so that at high drift velocities, the pattern was seen several times during the course of an experimental episode.

The response of the display oscilloscope to these analog control signals was calibrated with a silicon photocell. At typical mean operating levels, the response was linear up to ~ 40% contrast;[5] experiments were performed at total contrasts of < 35%. No attempt was made to calibrate the absolute intensity of the stimulus, because of the high variability of the optical density of the *Limulus* cornea between specimens.

The Biological Preparation

Adult horseshoe crabs, *Limulus polyphemus,* measuring 15–20 cm across the carapace, were obtained from Gulf Specimens Inc., Panacea, Fla. The animals were kept in filtered artificial seawater at 10° C. They were generally used within 6 wk of delivery, during which time they were not fed. Animals selected for use had "clear" eyes, with no perceptible abrasion of the cornea, and in an informal "neurological exam" they demonstrated brisk, vigorous flexion of the hinge muscle after noxious stimulation of the gill. In general, the speed and strength of the hinge muscle reflex appeared to correlate well with the health of the retina.

Recordings of neural activity were made using an *in situ* preparation (Corning et al. 1965; Biederman-Thorson and Thorson, 1971; Adolph, 1971; Kaplan and Barlow, 1975). In brief, the animal was secured to a wooden board on top of a manipulator which allowed the animal to be rotated and tilted. The gills were placed on a paper towel moistened with the seawater in which the animal had been living. The animals were always capable of vigorous motion when removed from the apparatus, often after as long as 18 h. A surgical trephine was used to cut a hole 2 cm in diameter in the carapace, about 3 cm anterior to the animal's right eye, above the optic nerve. The nerve was transected, dissected free, and pulled into a small recording chamber, which was then screwed into the carapace. The chamber was filled with seawater, and the nerve dissected with glass needles until a strand which contained a single functioning axon was obtained (Hartline and Graham, 1932). This strand was laid on a cotton wick-silver/silver chloride electrode. The signal from the electrode was amplified and filtered by a differential amplifier, and monitored via oscilloscope and loudspeaker.

The temperature of the crab was measured by means of a thermistor probe (Yellow Springs Instrument Co., Yellow Springs, Ohio) inserted in a hole placed medial to the animal's left eye. The animal's temperature was controlled by coupling it to a constant-temperature circulator (Lauda Div., Brinkmann Instruments, Inc. Westbury, N.Y.) with a modified ice-bag. Eye temperature was held at 22° C, and typically varied < 0.5° C over the course of a 10-h experiment. This elevated temperature was chosen because it raises the mean impulse rate (Adolph, 1973) and enhances the response to flickering light (Brodie, 1978).

Data Acquisition

The amplified signal from the wick electrode was converted to a train of uniform pulses by a discriminator. These pulses served as input to the PDP 11/45 computer, which

[5] Contrast = {(peak intensity) − (trough intensity)}/{(peak intensity) + (trough intensity)}.

recorded the successive intervals between impulses in a file on magnetic disk for later analysis. Resolution was 10^{-4} s, and the same clock was used to time impulse arrivals as was used to generate the time-varying stimuli. The uniform pulses were also used to drive a "hyperbolic sweep" monitor, which gave a visual indication of instantaneous rate. (This device employed a new digital design by M. Rossetto, and replaced the analog circuit of MacNichol and Jacobs, 1955).

Protocol

The experimental schedule consisted of 60-s periods of illumination in alternation with 90-s periods of darkness. This episode pattern was designed to maintain the eye in a uniform state of light adaptation, over the duration of the experiment, as estimated by the total number of neural impulses produced in each episode. Successive episodes alternated between the analysis stimulus (a sinusoidal grating in space modulated temporally by a sum-of-sinusoids signal) and the synthesis stimulus (a pattern of light drifting across the eye at a constant speed). A stimulus cycle consisted of 16 episodes: analysis episodes at each of eight spatial frequencies (1/10, 1, 2, 4, 8, 16, 20, and 32 cycles/eye width) interleaved with two presentations of the synthesis stimulus at each of four drift velocities, one presentation in each direction.

These stimulus cycles (which lasted 40 min) were repeated indefinitely until the nerve fiber ceased conducting impulses. Experiments typically lasted at least 6 h, and occasionally as long as 10 h. Nerve conduction failures were as a rule the result of the drying out of the exposed portion of the optic nerve; activity was readily obtained from more proximal portions of the nerve. We are thus confident that the retina did not significantly deteriorate over the course of an experiment.

Computations

All computations were based on data from the last 50 s of each 60-s episode, well after the initial on-transient had decayed. The spatiotemporal transfer function $\mathcal{F}(\xi, \omega)$ was obtained from the analysis episodes by means of a least-squares fitting algorithm, as described in Appendix B. This procedure is equivalent to ordinary discrete Fourier analysis of binned (histogram) data, with arbitrarily narrow bins; equivalently, it yields the spectrum of the impulse train interpreted as a series of δ-functions. The algorithm is particularly suited to the handling of pooled data from episodes with identical stimuli.

For each spatial frequency, the algorithm determines real numbers r_n so that the function $f(t) = \Sigma r_n f_n\ (t)$ best approximates the response $r(t)$ (in a certain least-squares sense; see Appendix B), where the f_n are the functions 1, $t - t_m$ (t_m is the midpoint of the data collection period), sin $\omega_m t$, cos $\omega_m t$, sin $2\omega_m t$, and cos $2\omega_m t$ (where the ω_m are the input frequencies). The coefficient of the function 1 gives the mean impulse rate over the episode; the coefficient of the function $t - t_m$ (the "ramp slope") describes the slow decay of the impulse rate over the course of an episode. As described above, these parameters are ignored in the remaining analysis, but are added back to the Fourier synthesis at the end of the calculation. The coefficients of the sin $\omega_m t$ and cos $\omega_m t$ terms determined the value of $\mathcal{F}(\xi,\omega_m)$ (where ξ is the spatial frequency of the stimulus which produced the particular data being analyzed): the amplitude of $\mathcal{F}(\xi,\omega_m)$ is the square root of the sum of the squares of these two coefficients, while the tangent of the phase of $\mathcal{F}(\xi, \omega_m)$ is given by their quotient. The coefficients of sin $2\omega_m t$ and cos $2\omega_m t$ measure nonlinearities in the response of the system. The entire set of coefficients was determined for the pooled data from all the analysis episodes at each spatial frequency.

The phase information for the transfer function at each spatiotemporal frequency pair (ξ_m,ω_m) was obtained, as described above, by taking the arctangent of a quotient; the

computer expressed these results as real numbers between $-\pi$ and π. These phase data were individually adjusted by a multiple of 2π so as to obtain continuous phase curves. Thus, values of $\mathcal{F}(\xi,\omega)$, as amplitude and phase, were obtained at the 64 spatiotemporal frequency points corresponding to all the possible combinations of the eight spatial and eight temporal frequencies present in the analysis stimuli. In order to estimate $\mathcal{F}(\xi,\omega)$ for (ξ,ω) between the points of the input lattice, a two-dimensional cubic spline was used. For this purpose, the transfer function data were expressed in terms of two separate real functions (log amplitude, and phase) of the variables log ξ and log ω. The complex transfer function $\mathcal{F}(\xi,\omega)$ was then reconstructed from the amplitude and phase.

To avoid artifacts due to abrupt frequency cutoffs, the transfer function was extrapolated beyond the spatiotemporal frequency lattice at which it had been measured. The extrapolation to high spatial frequency extended the observed attenuation of amplitude seen at spatial frequencies above 20 cycles/eye width; for each spatial frequency, the amplitude was fixed as a small constant multiple of the amplitude observed at the highest spatial frequency where measurements were made. Phases were extrapolated by setting them equal to the phases measured at the highest spatial frequency used. The Fourier syntheses were insensitive to the details of these high-frequency extrapolations. It was unnecessary to extrapolate to low spatial frequency, as the data extended down to 0.1 cycles/eye width. The high temporal frequency extrapolations were provided as approximate continuations of the typical observed high-frequency roll-off in amplitude and phase.

For the extrapolation to low temporal frequencies, the low-frequency transfer-function measurements of Biederman-Thorson and Thorson (1971) were used as a guide. Under experimental conditions quite similar to ours, they measured temporal transfer functions from 0.4 Hz down to 0.004 Hz. In this regime they found that the transfer function could be expressed as $\mathcal{F}(\omega) = K\cdot(i\omega)^p$ where p is a real exponent between 0.18 and 0.27 (mean 0.23), and K is a real constant of proportionality. For simplicity we adopted the exponent $p = 0.25$, and extrapolated the transfer functions accordingly, fixing the proportionality constant by the amplitude observed at the lowest frequency where measurements were available (0.1 Hz), and extrapolating the phase to the low-frequency phase lead of $\pi/8$ radians implied by the exponent $p = 1/4$. Although the very low frequency features of the Fourier syntheses were not insensitive to the details of the low temporal frequency extrapolation, this parameter-free procedure produced no systematic discrepancies between experiment and prediction in the very low frequency range.

The synthesis episodes were treated differently. The data from episodes with identical stimuli were averaged together by computing the instantaneous rate function $s(t)$ for each episode, and then averaging these functions on a mesh of 1,024 equally spaced points covering the 50-s episode length. The resultant averaged response function, $\sigma(t)$, was plotted on a digital plotter (CalComp 565, California Computer Products, Inc., Anaheim, Calif.) for later comparison with the Fourier syntheses.

The synthesis stimuli were presented in two directions at each velocity. As these pairs of stimuli consisted of reflections of each other about the test ommatidium, they served to verify our assumptions about the symmetry of the inhibitory fields, and to verify the accurate placement of the stimulus origin so as to coincide with the test ommatidium. In all cases but one, the responses to the two mirror-image stimuli appeared nearly identical (see Results, below). This observation permitted us to further increase the signal-to-noise ratio by averaging together all the synthesis episodes at each velocity, thus combining the response to each synthesis stimulus with the response to its mirror image.

The Fourier synthesis computations were done in Fortran complex arithmetic with the Fast Fourier Transform algorithm (FFT) on a mesh of 1,024 equally spaced points

covering the response to one full period of the periodic synthesis stimulus. (Thus, for rapidly drifting patterns, each experimental record provided several repetitions of the response to the moving stimulus. Except for the slow drift in mean impulse rate, these repetitions should, in principle, be identical.) The translation of the synthesis formula (Eq. 16′) (derived above in terms of Fourier integrals) into a form suitable for use with the (discrete) FFT is essentially straightforward. The computation consisted of filling an array with the transform of the stimulus pattern (obtained either analytically or by FFT), multiplying by the transfer function, and inverting by FFT.[6] The time-stationary (periodic) portion of the response was then available as the real part of this result. The mean impulse rate and "ramp" (describing the slow drift of the impulse rate over the course of an episode) were added to the periodic response, and the sum was plotted in a form compatible with the plots of the averaged synthesis episodes for direct visual comparison. This calculation was repeated for each stimulus drift velocity.

We wish to emphasize that this entire calculation, from the measurements of the transfer function to the calculation of the Fourier synthesis prediction, allowed no adjustment of free parameters. The prediction is explicitly and unambiguously determined by the measured transfer function, mean impulse rate, and ramp slope.

RESULTS

The outcome of the analysis portion of the protocol is depicted in Figs. 2 and 3. Fig. 2 shows the average instantaneous rate function $\sigma(t)$ for the response to a typical analysis episode. It is important to note that, contrary to its noisy appearance, such a record is in fact a definite response to a fixed temporal signal, albeit a harmonically rich signal. In Fig. 3, the marked dependence of the response on the spatial frequency of the analysis stimulus is illustrated. At low spatial frequencies, a moderate response to the temporal modulation of the stimulus is observed. As the spatial frequency is increased, an increase in the response to flicker is apparent. The peak sensitivity is around four cycles/eye width. At high spatial frequencies, the response decreases, until, at 32 cycles/eye width it is essentially undetectable. It may be noted that, as all the analysis episodes share a common temporal modulation signal, the records at different spatial frequencies show corresponding features at corresponding time points.

These effects are specified quantitatively in Fig. 4, which shows the full spatiotemporal transfer function derived from the same preparation as in Fig. 3. Though the general trend of the curves agrees with the description above, the following features may be noted. The relative sensitivity of the eye to sine-wave gratings of differing spatial frequency depends strongly on temporal frequency. Thus, at low temporal frequency, the response is greatest at intermediate spatial frequency falling off gently at low spatial frequency, and sharply at high spatial frequency. At intermediate temporal frequency, the eye

[6] Because of the phenomenon of "aliasing," the FFT may be interpreted equivalently as operating either on the array of frequencies $0, \xi, 2\xi, \ldots, (2^N - 1)\xi$, or on the array $0, \xi, 2\xi, \ldots, 2^{N-1}\xi, -(2^{N-1} - 1)\xi, -(2^{N-1}-2)\xi, \ldots, -2\xi, -\xi$. For our purposes, the second interpretation is the correct one, because the power in the negative-frequency components greatly exceeds that in the positive high-frequency components, due to the high-frequency cutoff of both the stimulus $\mathcal{S}(\xi)$ and the transfer function $\mathcal{F}(\xi, -\xi\nu)$. The transfer function for negative frequencies is obtained from the symmetry relations (Eqs. 17–19).

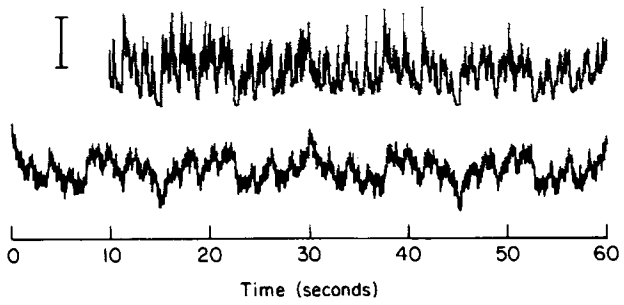

FIGURE 2. Response of test ommatidium to temporally modulated sine-wave grating. The bottom record shows the sum-of-sinusoids temporal signal used to modulate a sinusoidal grating stimulus over each 60-s episode. The top record shows the average instantaneous rate response $\sigma(t)$ from 14 repetitions of such an analysis stimulus, with a spatial frequency of 4 cycles/eye width. The data from the first 10 s of each episode were discarded to avoid the effect of the initial on-transient. Scale marker: 10 impulses/s.

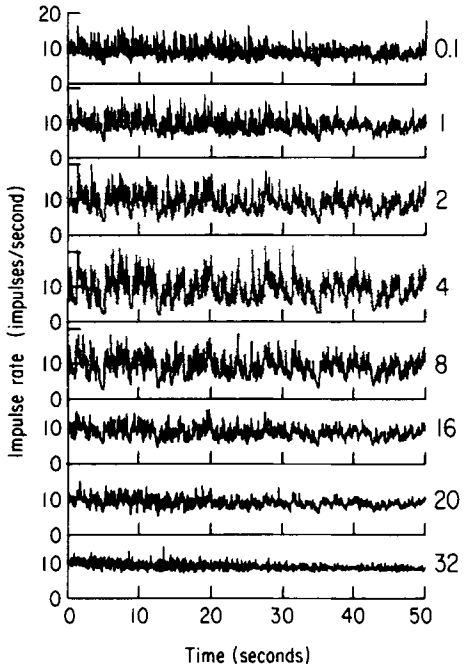

FIGURE 3. Effect of spatial frequency on response to temporally modulated sine-wave gratings. Each record is the average of 14 episodes. The stimulus consisted of a sinusoidal grating (spatial frequencies shown at right) placed with a peak centered over the test ommatidium, modulated according to the temporal signal shown in Fig. 2.

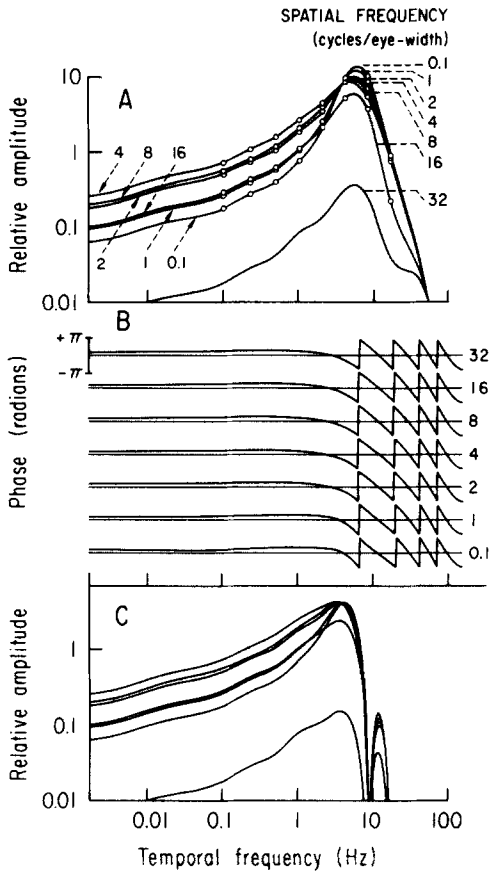

FIGURE 4. Spatiotemporal transfer functions for the preparation of Fig. 3. (A) Bode plots (log amplitude vs. log frequency) of the fractional modulation of the mean impulse density $r(t)$ for each spatial frequency. The points indicated (O) were obtained from experimental measurements; the remaining portions of the curves were extrapolated as described in the text. (This preparation produced no detectable response at 32 cycles/eye width (see Fig. 2). As a curve for this spatial frequency was needed for computational purposes, it was extrapolated by setting the amplitude at 32 cycles/eye width equal to 10% of the amplitude measured at 20 cycles/eye width.) (B) Phase vs. log frequency is indicated (modulo 2π) on a separate axis for each spatial frequency. The curves were extrapolated in the same regions as the amplitudes, above. (C) The transfer function amplitudes for the same preparation, in terms of the mean instantaneous rate function $\sigma(t)$, obtained by multiplying the transfer function in (A) by the transfer function $|B(\omega, \nu)|^2$ (see text). The small undulations of the amplitude curves (A) and (C) at low frequency are artifacts of the extrapolation procedure.

is most responsive at low spatial frequency, with response decreasing monotonically with increasing spatial frequency. At high temporal frequency, there is little dependence on spatial frequency, except for the ultimate high-frequency cutoff. These findings may be considered the analog, with sine-wave gratings,

of the more familiar "small spot/large spot" experiments (Ratliff et al., 1967; Ratliff et al., 1969; Knight et al., 1970).

The spatial dependence of the phase of the transfer function is more subtle, with detail concentrated at the lower temporal frequencies. The low-frequency phase lead is slightly greater at low spatial frequencies and persists to higher temporal frequencies. Once it starts, however, the rate of increase of the phase lag with temporal frequency is greater at low spatial frequency, so that there is little difference in the phase lags seen at all spatial frequencies at high temporal frequency. The full implications of the transfer function measurements are discussed at greater length in the following article (Brodie et al., 1978).

As was discussed above, the Fourier syntheses were computed in terms of the mean instantaneous rate output variable $\sigma(t)$. For this purpose, the transfer function amplitudes, measured in terms of the mean impulse density, $r(t)$, were multiplied by the correction factor $|B(\omega, v)|^2$. The corrected amplitudes are shown in Fig. 4 C. The effect of the correction is mainly to attenuate the response at frequencies above the mean impulse rate. The phases are, of course, unchanged.

Typical averaged responses from the synthesis portion of the protocol are shown at the top of Fig. 5. For the experiment shown, the synthesis stimulus consisted of a square wave of spatial frequency 0.5 cycles/eye width, which was moved slowly across the eye. Because the stimulus was viewed by the animal through an effective "window" one eye width across, the stimulus had the appearance of a "step" of light intensity advancing across the screen. As the records from such mirror-image presentation of the stimulus are, in general, nearly identical, we have deemed it appropriate to average together all such responses. Such an averaged response is shown in the bottom of Fig. 5; the

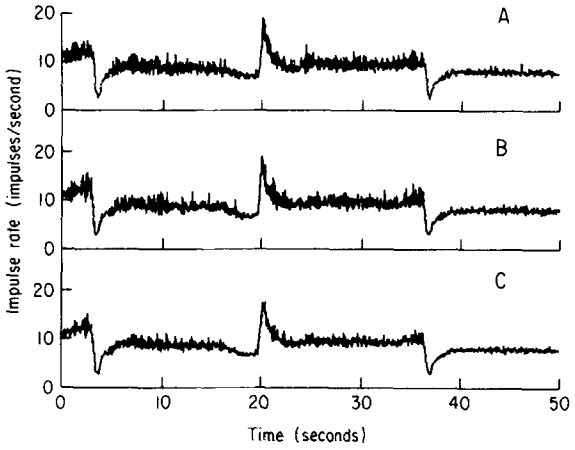

FIGURE 5. Comparison of the response to mirror-image stimuli. The top two records show the average instantaneous rate response $\sigma(t)$ obtained from 14 presentations of a drifting edge stimulus moving with drift velocity (A) +0.06 eye widths/s or (B) −0.06 eye widths/s. The record (C) is the averaged response of all 28 episodes. The preparation is the same as used in Figs. 3 and 4.

improvement in signal-to-noise ratio is evident. The features seen in this record, while to some extent dependent on the drift velocity of the stimulus (here, 0.06 eye widths/s), are common to such step-responses (see below). Of particular interest are the anticipatory "Mach bands"[7] of excitation or inhibition that precede the crossing of the test ommatidium by the moving edge. The crossing itself is seen as a clear on- or off-transient, which then decays, sometimes with a small overshoot, as here. In the intervals between the step transients, the impulse rate settles to a steady-state value. This value is nearly the same, regardless of whether the steady state is a response to the bright or dim region of the step-pattern stimulus.

An example of the effect of an asymmetrical inhibitory field on such records is seen in Fig. 6. In this preparation, the test ommatidium was located within 2 mm of an edge of the eye, and thus received manifestly asymmetrical input

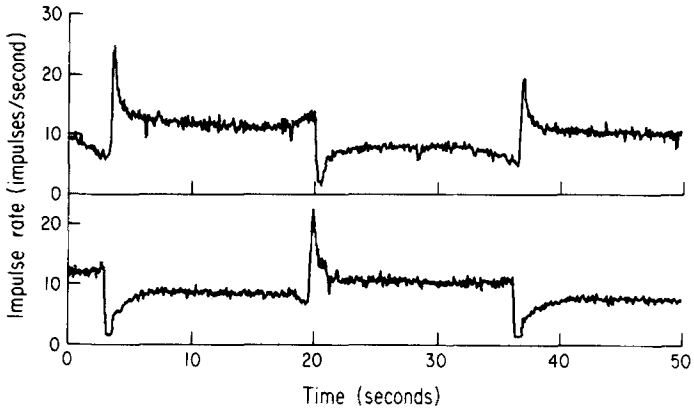

FIGURE 6. Step-transient responses of an ommatidium with an asymmetric inhibitory field. The test ommatidium in this preparation was located within a few ommatidia of the posterior edge of the eye. The anticipatory Mach bands were much more pronounced when the step stimulus moved toward that edge of the eye (top record) than when the stimulus moved away from the edge (bottom record).

from the rest of the retina. Thus, a Mach band typical of the drift velocity (0.06 eye widths/s) is seen when the steps drift toward the edge of the eye, while steps drifting away from the edge can affect very few ommatidia before encountering the test ommatidium, and thus they are scarcely anticipated. Such ommatidia were scrupulously avoided in the rest of the study. Hence, all further figures depicting responses to moving stimuli display the average of responses to mirror-image stimuli without further comment.

The records from synthesis episodes at four different drift velocities are shown in Fig. 7. The responses show a marked dependence on the drift velocity

[7] Strictly speaking, the term "Mach bands" refers to the maxima and minima seen in a static stimulus pattern consisting of a gradient of intensity between two uniform areas of different intensity (see Ratliff, 1965). We use the term loosely here to include the maxima and minima in neural responses to stepwise changes in intensity.

of the stimulus. At very low speeds the step in light intensity takes a significant time to cross the test ommatidium, and there is only a modest transient response to the step stimulus. This transient decays monotonically to a steady response. As the velocity is increased, the transient responses increase dramatically, momentarily driving the unit at over three times its average impulse rate. The inhibitory precursors are somewhat strengthened, but, of course, occupy a shorter interval of time. Immediately after the on-transient responses, the

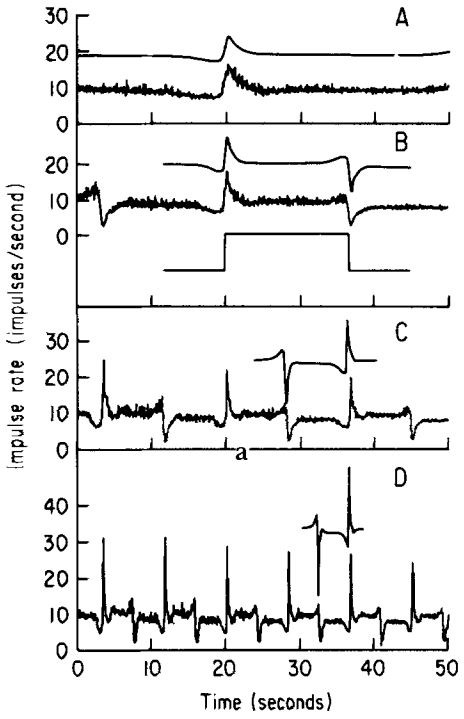

FIGURE 7. Fourier synthesis of step-transient responses. The figure shows the observed averaged response $\sigma(t)$ to drifting steps of light intensity (same preparation as Figs. 3, 4, and 5). Drift velocities were (A) 0.03, (B) 0.06, (C) 0.12, and (D) 0.24 eye widths/s. The episodes at the slowest speed provided only one on-transient; the others provided at least one full cycle of the stimulus. The curves offset immediately above the observed records are the predictions, for one cycle of the stimulus, of the Fourier synthesis procedure described in the text, applied to the spatiotemporal transfer function shown in Fig. 4. The intensity of the stimulus at the test ommatidium is shown for one stimulus cycle in (B).

impulse rate falls rapidly, overshooting the subsequent steady response to the bright portion of the step. At high velocity, the off-transients, which would have to extend to "negative" impulse rates to mirror the observed on-transients, are severely truncated.

The predictions of the Fourier synthesis procedure (using the transfer-function data from Fig. 4 B and C) are shown above the experimental records.

The agreement between the Fourier predictions and the experimental records is, on the whole, excellent. The linear theory successfully predicts the form and height of the step transients (a sensitive function of drift velocity), and the width and strength of the Mach bands. The limited dependence of the "steady state" response on the intensity of the illumination between step transients is also correctly predicted by the Fourier synthesis calculation.

The synthesis shows only a few systematic discrepancies from the actual responses. The slight overshoot of the response at intermediate velocities is somewhat underestimated, and the sculpturing of the on-transient at the lowest velocity is slightly distorted. The biggest discrepancy is the truncation of the off-transients at high drift rates. This highly nonlinear phenomenon is beyond the scope of our linear theory. The truncation also produces secondary effects, such as the absence of overshoot after high-speed off-transients, which likewise are not predicted by the Fourier synthesis.

We have obtained results comparable to those shown above on several other preparations. Further evidence of the extent to which our transfer function measurements characterize the response of a *Limulus* eye to moving stimuli was also obtained.

Figs. 8 and 9 show the results of an analysis-synthesis experiment performed on a *Limulus* with weak and sluggish reflexes; this specimen would not have been used had a healthier one been available. The transfer function shows better optical resolution than that of Fig. 4, with a readily measurable response at 32 cycles/eye width, but very little dependence on spatial frequency. This apparent lack of lateral inhibition is confirmed by the synthesis records, which show virtually no Mach band effects at all. Nonetheless, the agreement between the Fourier synthesis and the experimental records is striking, at velocities ranging over an order of magnitude. It thus appears that our transfer function

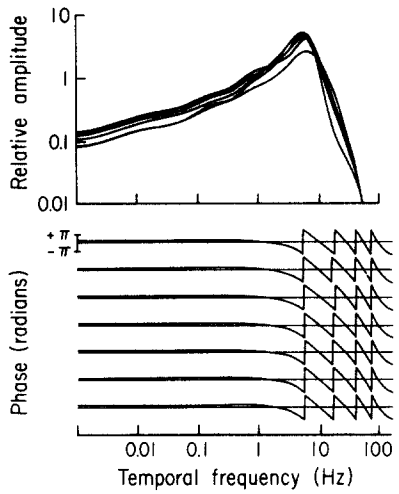

FIGURE 8. Transfer function for a "sick" *Limulus*. Bode plots of measured spatiotemporal transfer function, plotted as in Fig. 4. At the peak, amplitudes decrease monotonically with increasing spatial frequency.

measurements accurately describe the dynamics of even a somewhat pathological eye.

We have also performed syntheses of the response to drifting patterns other than steps. Figs. 10 and 11 show the results of a synthesis of the response to the "step complement" stimulus of Ratliff and Sirovich (1978). This stimulus, which

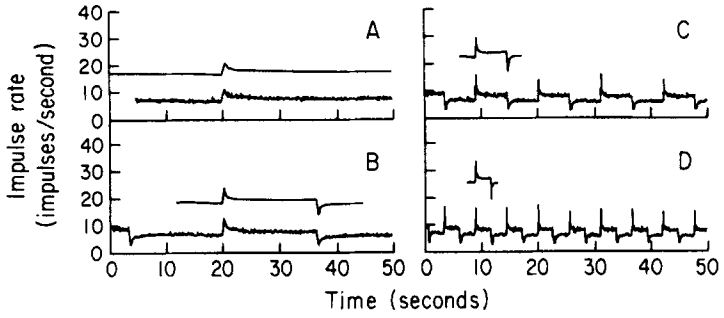

FIGURE 9. Fourier synthesis for "sick" *Limulus* (same preparation as Fig. 8). Predicted and measured responses (averages of eight episodes) to drifting step stimuli are plotted as in Fig. 7. Drift velocities were (A) 0.03, (B) 0.06, (C) 0.18, and (D) 0.36 eye widths/s.

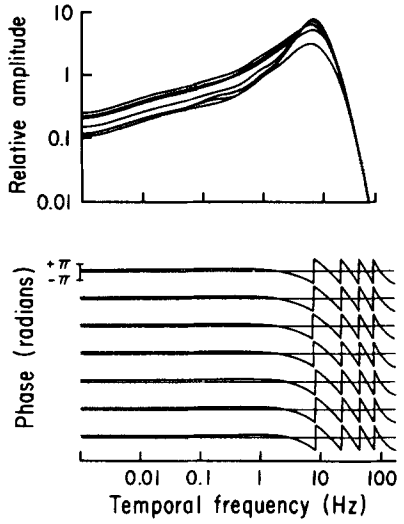

FIGURE 10. Transfer function for experiment of Fig. 11. At peak, amplitudes decrease monotonically with increasing spatial frequency.

is composed of a sinusoid of the lowest possible frequency (0.5 cycles/eye width) plus a fast exponential decay superposed on a step, is designed to resemble the step stimulus as little as possible, yet produce similar visual responses. Even though the stimulus possesses no sharp dicontinuities, the response clearly resembles the typical response to true drifting steps, especially at low velocities.

At higher speeds, the eye readily perceives the 0.5 cycles/eye-width sinusoid. All of these responses, up to a velocity of 0.8 eye widths/s, are well predicted by the Fourier synthesis. With the measured spatiotemporal transfer function, we can perform a Fourier synthesis to predict the response of this preparation to a true step stimulus, such as the one used for the experiments of Figs. 7 and 9. These predictions are shown in Fig. 12, for comparison with the response to the step-complement stimulus.

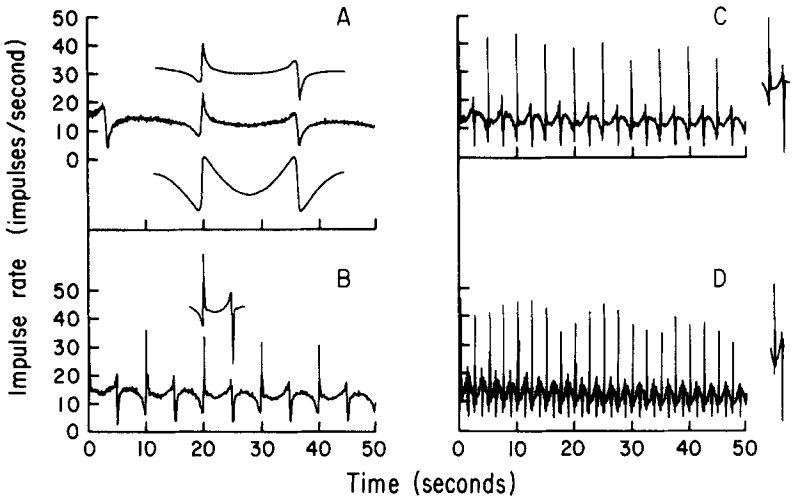

FIGURE 11. Predicted and measured responses to moving "step complement" stimulus. One cycle of the stimulus is reproduced as the bottom record in (A). Drift velocities were (A) 0.06, (B) 0.20, (C) 0.40, and (D) 0.80 eye widths/s. Measured responses are the average of 12 episodes.

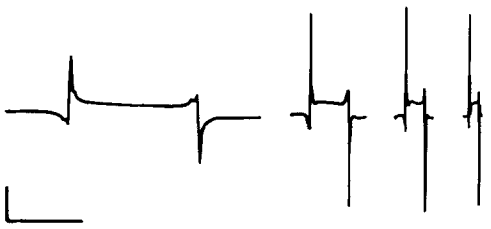

FIGURE 12. Predicted step responses for preparation of Figs. 10 and 11. Drift velocities, from left to right: 0.06, 0.20, 0.40, 0.80 eye widths/s. Scale marker: horizontal, 10 s; vertical, 10 impulses/s.

As a final test of the ability of our procedure to handle "arbitrary" stimuli, we produced a visual stimulus whose light-intensity profile resembles a row of buildings. The results of an experiment using this stimulus are shown in Figs. 13 and 14. The agreement between the predicted and measured responses is again excellent.

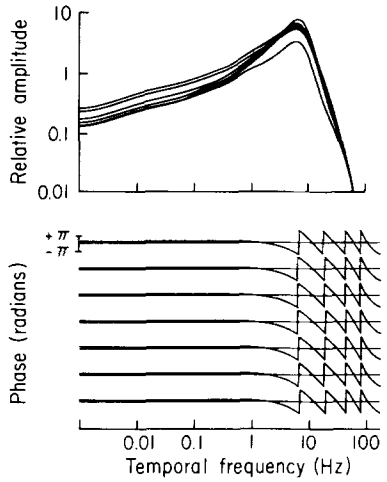

FIGURE 13. Transfer function for experiment of Fig. 14.

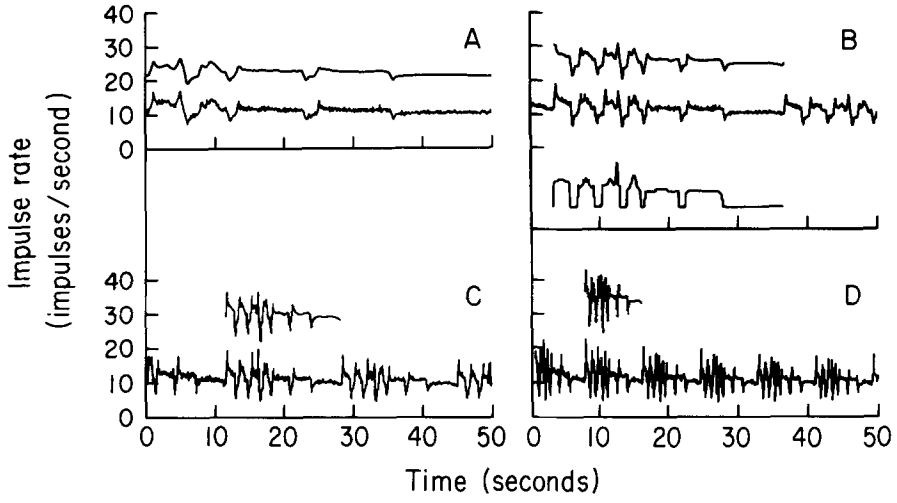

FIGURE 14. Predicted and measured responses to moving "arbitrary" stimulus. One cycle of the stimulus is reproduced as bottom record in (B). Drift velocities were (A) 0.03, (B) 0.06, (C) 0.12, and (D) 0.24 eye widths/s. Measured responses are the average of 22 episodes.

DISCUSSION

The extensive agreement between the measured responses to moving stimuli and the predictions of our Fourier-synthetic calculations demonstrates the essential validity of our program of linear systems analysis. Though the major assumption of linearity is known to hold for many aspects of the *Limulus* visual transduction, especially in the vicinity of a fixed operating point, there are important known exceptions, such as the dependence of inhibitory coupling on

excitation levels, and the phenomenon of inhibitory thresholds. Our results confirm that, in spite of these potential complications, the *Limulus* system responds with linear behavior well beyond the range of small perturbations.

The only striking nonlinear effect demonstrated in our study is the truncation of off-transients corresponding to the limitation of the pulse-coding scheme. Our data appear to be consistent with the hypothesis that, under the conditions of widespread illumination and moderate impulse rate, the effective threshold for lateral inhibition (at least for inhibitory transients) is the absolute threshold: the absence of impulses in the inhibiting units. This may be a small limitation in practice: those stimuli in which features which greatly exceed the intensity of the mean illumination are brief and well separated from each other (such as the stimulus of Fig. 14) produce little or none of this truncation effect, especially at low stimulus velocities.

This study provides verification of the behavior of large numbers of interacting neurons in the dynamic situation. We confirm the presence of Mach bands which precede waves of excitation moving across the eye. The relative insensitivity of the *Limulus* retina to slowly changing, or slowly moving, stimuli has been definitively demonstrated. As has often been stated elsewhere, such response characteristics have the effect of accentuating contours and movements in the information passed by the eye to the brain. On the other hand, it should be pointed out that for moderately rich stimuli, the *Limulus* eccentric cell provides a fairly accurate depiction of the stimulus at even rather leisurely drift velocities.

We thus conclude that the spatiotemporal transfer functions, as measured above, in fact serve as concise complete characterizations of the *Limulus* visual system in the regime studied, and therefore that the properties of a *Limulus* retina are well specified by the retina's response to sinusoidal gratings modulated sinusoidally in time. In principle, then, the task of the *Limulus* visual physiologist may be reduced, to a large extent, to predicting and explaining the various features of the measured transfer functions.

APPENDIX A

A Fiber-Optic "Contact Lens" for the *Limulus* Lateral Eye

The ommatidia of the *Limulus* lateral eye, which have an acceptance angle of <6°, diverge greatly, covering roughly a hemisphere of solid angle. A consequence of this geometry is that a stimulus consisting of parallel rays of incident light will excite only a small patch of ommatidia (corresponding to the pseudopupil seen from the direction from which the light comes). This has proved to be a scant impediment in studies involving only a few (or a few groups of), nearby ommatidia, where fiber-optic light guides less than a few millimeters in diameter have provided adequate stimuli. On the other hand, it has been very difficult to provide carefully controlled illumination to a large population of ommatidia. One approach to this problem is to place a naked *Limulus* eye close to a display oscilloscope.[8] Although this method has the advantage of great simplicity, it is capable of illuminating only about one-third of the horizontal extent of the eye. The resolution of the "natural optics" is also somewhat limited. Much better resolution can be obtained by imaging a stimulus directly onto the *Limulus* cornea with a

[8] Dodge, F., and E. Kaplan. Personal communication.

system of lenses. Unfortunately, this successfully illuminates only a small cluster of ommatidia. What is needed is an arrangement of light guides arranged along a curved surface resembling the *Limulus* cornea, whose optic axes converge in a manner corresponding to the divergence of the ommatidial axes.

To approximate such an optical array, we have turned to the technology of fiber-optic tapers. Such a taper consists of a frustum-like portion of a "coherent" lattice of glass fibers embedded in a glass matrix of lower refractive index, which has been heated and drawn into a conical shape. Ordinarily, the two end surfaces of such a taper are polished into parallel planes. The taper then maps each point of one surface to one point of the other surface, so that an image formed on one surface is reproduced on the other. Such tapers are routinely used as magnifiers or "condensers" (image reducers) (see Fig. A1 A) (Kapany, 1967). Unfortunately, if the narrow end of such a taper is simply ground to form a concave spherical surface conformable to the *Limulus* cornea, the optic axes of the fibers in the taper remain parallel to the axis of the cone, and to each other; they are thus poorly oriented to illuminate the divergent ommatidia in a *Limulus* eye.

Recently, we have obtained (courtesy of Walter P. Siegmund, Fiber-Optics Division, American Optical Corp., Southbridge, Mass.) fiber-optic tapers with concave spherical

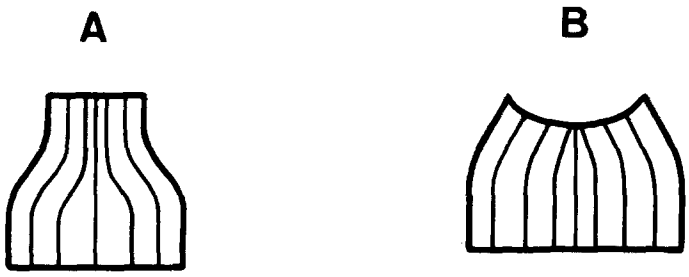

FIGURE A1. Schematic indication of the fiber orientation in two kinds of fiber-optic taper. (A) Standard magnifier/condenser: fibers perpendicular to two flat surfaces. (B) Fiber-optic taper used for these studies. Note how fibers are approximately normal to curved surface.

small ends (and flat large ends) fabricated so that the optic fibers are approximately perpendicular to the polished spherical surface (Fig. A1 B). Although such an array of fibers diverges somewhat less than the array of *Limulus* ommatidia, we have found that it satisfactorily illuminates virtually the entire *Limulus* eye. Inasmuch as these tapers provide the crucial link in the production of our visual stimulus, we describe them below in considerable detail.

The tapers (Fig. A2) are 2.8 cm in maximum diameter and 1.8 cm in height. The narrow ends are ground to spherical surfaces of different curvatures to accommodate eyes of various sizes. One taper was used for almost all the experiments, and is well suited to the eyes of most crabs of diameter 15–20 cm; it bears a spherical surface 1.2 cm wide and 0.25 cm deep, with a radius of curvature of about 0.85 cm. A second taper was used for a few crabs with large, flat eyes. Its spherical surface is 1.4 cm wide, 0.2 cm deep, with a radius of curvature of 1.3 cm. A third taper, designed for small eyes (spherical surface 1.0 cm wide, 0.3 cm deep, radius of curvature 0.57 cm), was not used.

The optical fibers of the tapers are roughly square in cross section. At the flat surface of each taper, they are 10 μm square; on the spherical surface, they are roughly 5 μm square (Fig. A3). As each ommatidium presents a corneal aperture approximately 200

μm in diameter, it is clear that in no significant way do the discrete fibers of the fiber-optic taper degrade the visual stimulus.

A more serious source of distortion stems from the geometric consequences of mapping a plane surface continuously onto a portion of a sphere. In any such mapping, some distortion is inevitable (Gauss, 1828). In our tapers, the distortion is modest and continuous (see Fig. A4), and was ignored in the experimental work, without apparent difficulty.[9]

The fiber-optic tapers were coupled to the *Limulus* eyes, both optically and mechanically, by gluing them directly to the cornea with a quick-setting, transparent cyanoacrylate glue (Krazy Glue, Chicago, Ill.). This provided an extremely stable linkage, with excellent optical properties (see below). Before the dissection was performed, projecting ridges on the *Limulus* carapace were removed with a rapidly rotating burr, and the

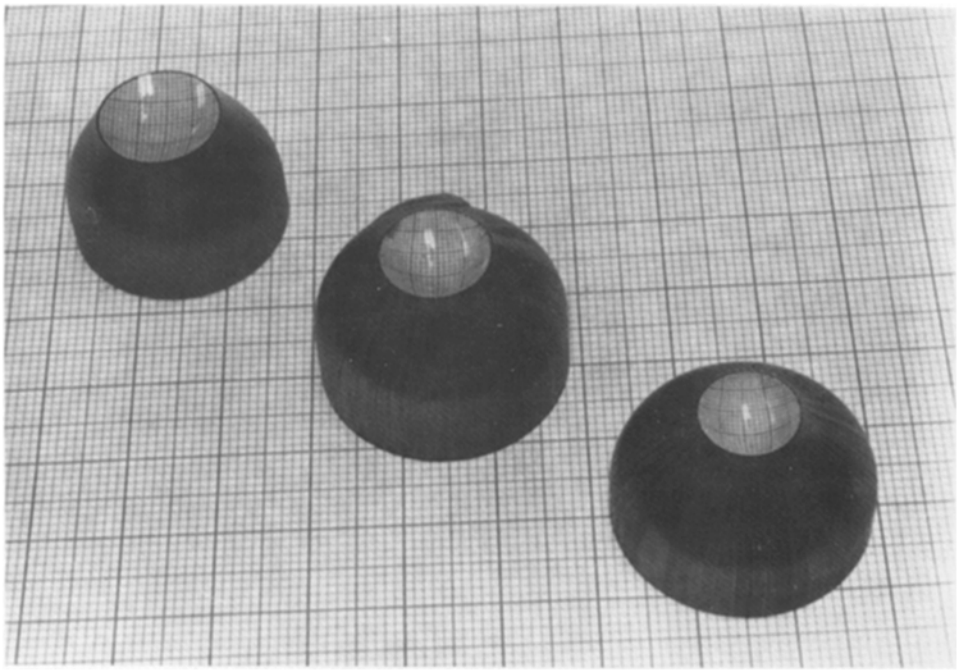

FIGURE A2. Three fiber-optic tapers obtained for this study; from left to right for large, medium, and small eyes, respectively.

appropriate size fiber-optic taper was selected. After the dissection, two drops of glue were placed on the concave surface of the taper, which was then immediately applied to the cornea, and held there by hand for 1 min. Once the taper was secured in this manner, the lattice of ommatidia was clearly visible on the flat surface of the cone (Fig. A5), and the neural response to test lamps was typically as vigorous as before the taper had been applied.

[9] If we regard the linear system under study as the fiber-optic cone followed by the *Limulus* retina, it is clear that the optical distortion does not invalidate the linear synthesis of the response of one test ommatidium. If severe, such distortion could, however, complicate the physiological interpretation of the measured transfer function; in the present study, we believe this effect to be unimportant.

Even though all experimental test ommatidia were chosen from the central region of the eye, it was evident that the fiber-optic taper was easily able to stimulate even very peripheral ommatidia, including those which ordinarily look along the carapace. We are thus confident that our stimulus effectively excited ommatidia across the entire width of the eye.

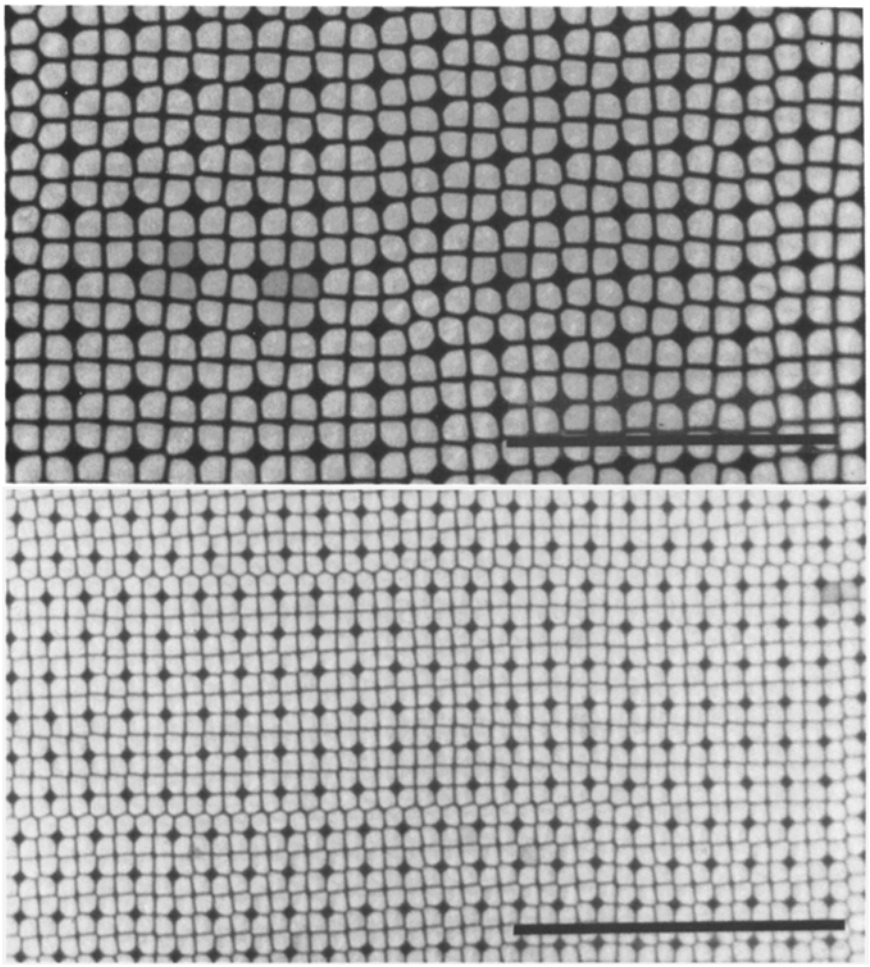

FIGURE A3. Top: photomicrograph of the fiber array at the flat surface of fiber-optic taper. The transmitting fibers are light, the matrix appears dark. Bottom: photomicrograph of the fiber array at the spherical surface of fiber-optic taper. Each fiber occupies roughly one-fourth of its previous area. Scale markers = 100 μm.

The image of the pattern produced on the display oscilloscope was focussed onto the flat surface of the fiber optic taper by a suitably mounted camera lens (Nikon Nikkor, f/1.2, 55 mm focal length). The overall effect of the combined optical system was to convert a pattern 15 cm wide and 2 cm high on the oscilloscope face to an image one eye-

width (~1 cm) wide and 0.13 eye-widths high (approximately five ommatidial diameters, or one-fourth of the height of the eye) on the *Limulus* cornea.

To evaluate the optical performance of this system, we examined its "point spread" characteristic, that is, the size of the image of a point light source. Of course, the ultimate performance of this system is limited by the discrete nature of the *Limulus* eye: the image of a point can be no smaller than a single ommatidium. To see if the image was any larger, we employed two methods. One method consisted of carefully removing the tissue behind the corneas of excised *Limulus* eyes, exposing the array of crystalline cones,

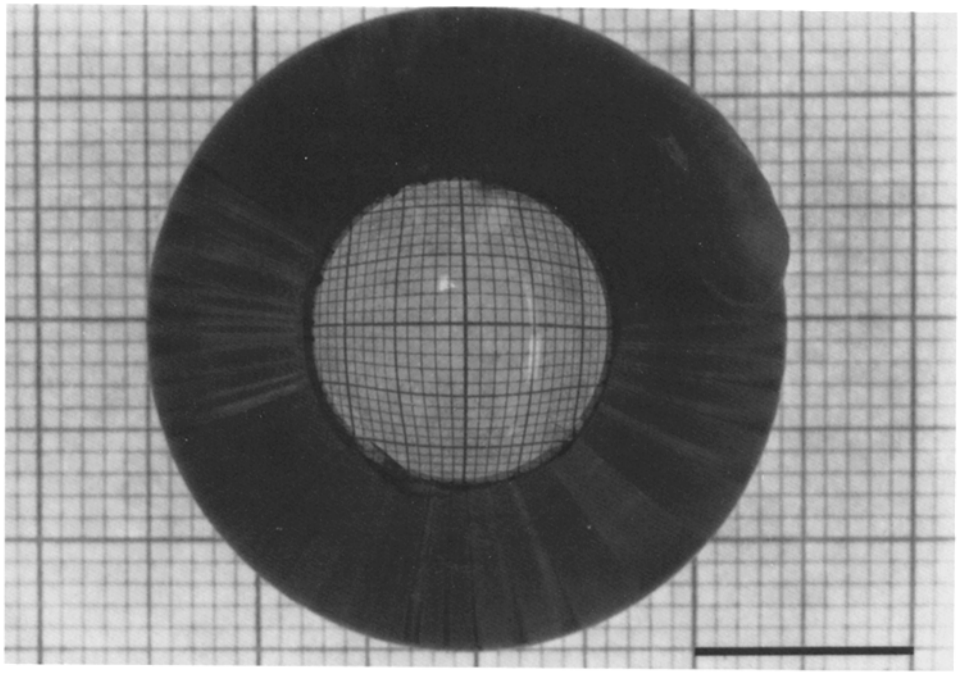

FIGURE A4. Continuous distortion produced by fiber-optic taper mapping from flat surface to spherical surface. The medium-radius taper, used in most experiments, is seen from above, resting on uniform graph paper. The distortion at the edges of the cone is slightly exaggerated by photographic foreshortening of the spherical surface. Scale marker = 1.0 cm.

and visually examining the image presented to the light-sensitive cells. The second method employed the comparison of transfer functions (light-to-impulse rate) for single ommatidia illuminated first by a small fiber-optic light guide and then by the smallest spot obtainable with our oscilloscope-lens-fiber-optic taper system. These experiments are described below.

To expose the crystalline cones, a *Limulus* eye was removed from the animal along with a rectangular section of the surrounding carapace, and placed in a vice. A rapidly rotating burr was used to remove most of the hard materials behind the eye; the remaining covering was removed with forceps. The soft tissues behind the cornea were then wiped away with a cotton-tipped applicator, leaving the array of crystalline cones

exposed. The eye was then glued to the fiber-optic taper in the usual way, and studied from behind with a stereoscopic dissecting microscope.

The simplest way to describe the point spread characteristic is to observe the image of a point source. When such a source was positioned at the center of an ommatidium, that crystalline cone was observed to glow brightly. A faint glow was seen in the six nearest-neighbor crystalline cones, and in no others. Unfortunately, this pattern proved unsuitable for photography. A more dramatic illustration of this same effect can be seen by examining the image of an edge; such an image is shown in Fig. A6. Though interpretation is hampered somewhat by the irregularity of the ommatidial array, the

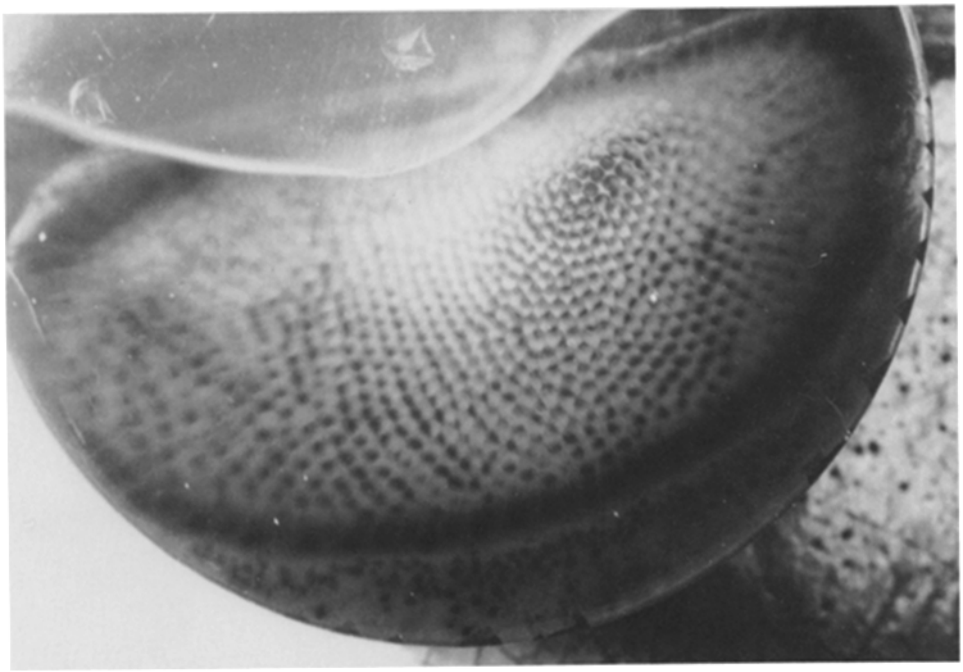

FIGURE A5. Lattice of ommatidia as seen through the fiber-optic taper. The meniscus at the top of the eye is the upper limit of the glue which couples the taper to the corneal surface. Test ommatidia were selected only from the central region of the eye, where the optical resolution was best.

figure clearly demonstrates that the edge is spread over no more than one ommatidial diameter. Fig. A7 shows a *Limulus*-eye view of a sinusoidal grating of ~4 cycles/eye. The physiological observation that even peripheral ommatidia are well illuminated is clearly demonstrated. Fig. A8 shows the image of a grating of roughly 10 cycles/eye. It is well resolved by the ommatidial array. Gratings at higher spatial frequencies were also observed, and were resolved up to 16 or 20 cycles/eye. These gratings were often difficult to see as static patterns, but drifting or counterphase modulation readily demonstrated their presence to the human observer. Beyond 20 cycles/eye, the Nyquist cutoff effect became prominent, and drifting gratings began to "beat" against the ommatidial lattice. (Recall that the eye is only 40 ommatidia wide.) These observations confirm our claim that the optical performance of this system is close to the limit imposed by the discrete nature of the eye itself.

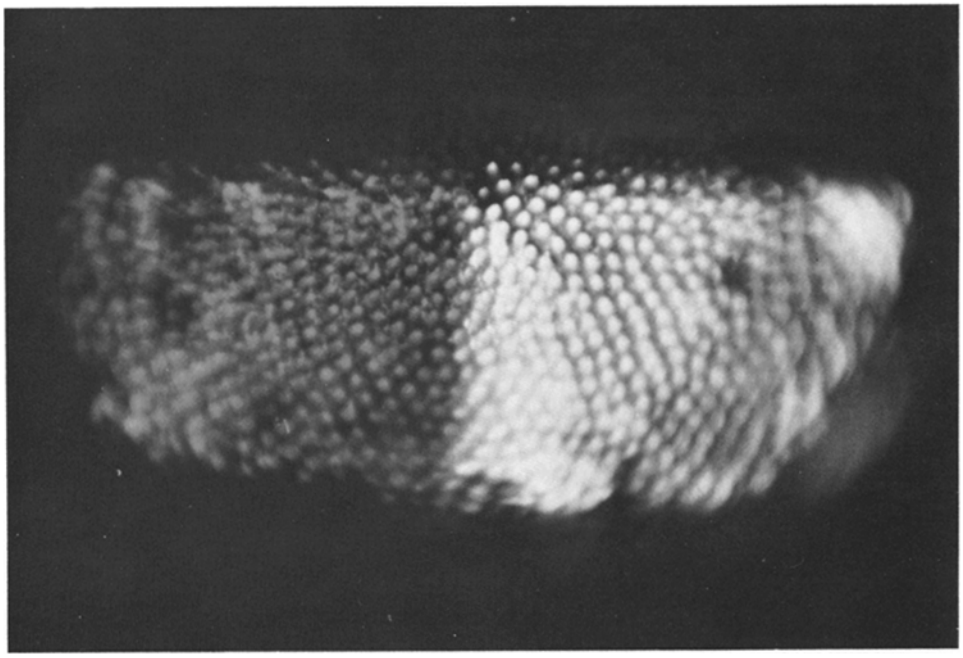

FIGURE A6. "Limulus-eye view" of an edge stimulus. The photograph shows the interior surface of the array of crystalline cones, illuminated from the corneal surface by the optical system described in the text. The sharp edge is degraded by no more than the width of a single ommatidium. The entire eye is ~1 cm wide.

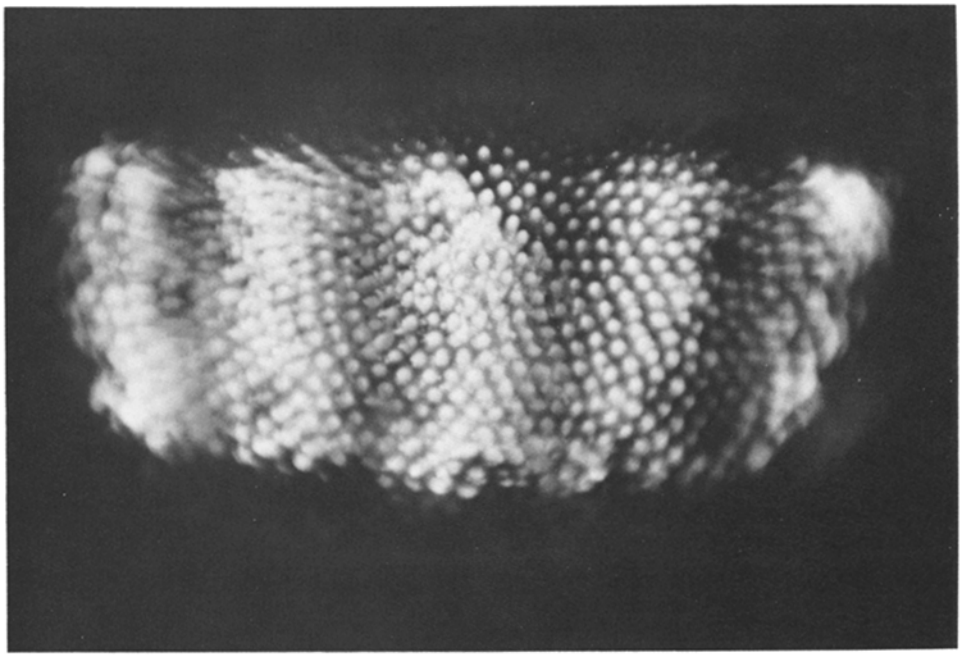

FIGURE A7. Crystalline cone image of sinusoidal grating, 4 cycles/eye width.

Our second method of checking the point spread of the optics was more physiological than the first. We performed, in essence, a "small spot/large spot" experiment (Ratliff et al., 1967), reasoning that if our optical system significantly degraded the image of a point into a spot illuminating the ommatidia surrounding the test ommatidium, then the light-to-impulse rate transfer function for this optical system should show a "tuning" effect, as compared to the transfer function produced by true point-source illumination (Ratliff et al., 1969), as provided by a fiber-optic light-pipe (Barlow, 1967). We therefore measured the transfer function of a test ommatidium illuminated by a 76 μm diameter light-pipe placed on the cornea. The light source was a glow-modulator tube, operated as described elsewhere (Knight et al., 1970), and driven by a computer-generated sum-of-sinusoids signal. After this measurement, a fiber optic taper was glued to the cornea. The same

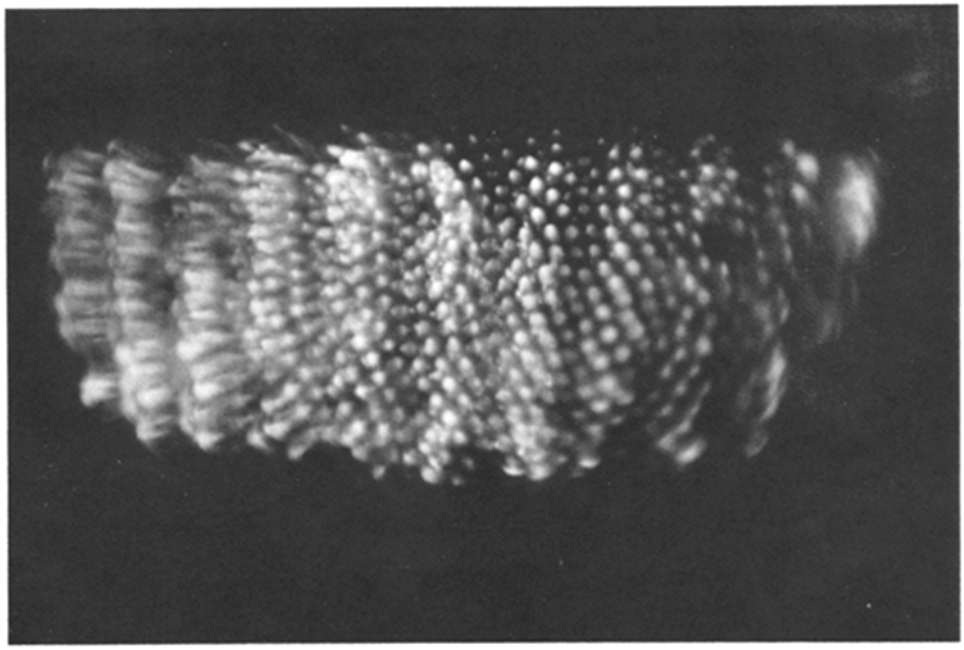

FIGURE A8. Crystalline cone image of sinusoidal grating, 10 cycles/eye width.

computer-generated signal used above was used to drive the oscilloscope, and the transfer function of the same test ommatidium, now illuminated with our fiber-optic taper optical system was measured. The f-stop diaphragm of the camera lens was used to adjust the mean impulse rate to approximately equal that obtained with light-pipe ilumination.

Typical data are shown in Fig. A9. The curves for both amplitude and phase agree to well within the tolerance required by the slight drift of the preparation over the duration of the experiment (in this case, ~2½ h). We conclude that the fiber-optic taper optical system does not significantly degrade the point spread characteristic of the intrinsic *Limulus* optics.

A more quantitative approach to the measurement of the *Limulus* optical point spread characteristic is described in the following paper (Brodie et al., 1978).

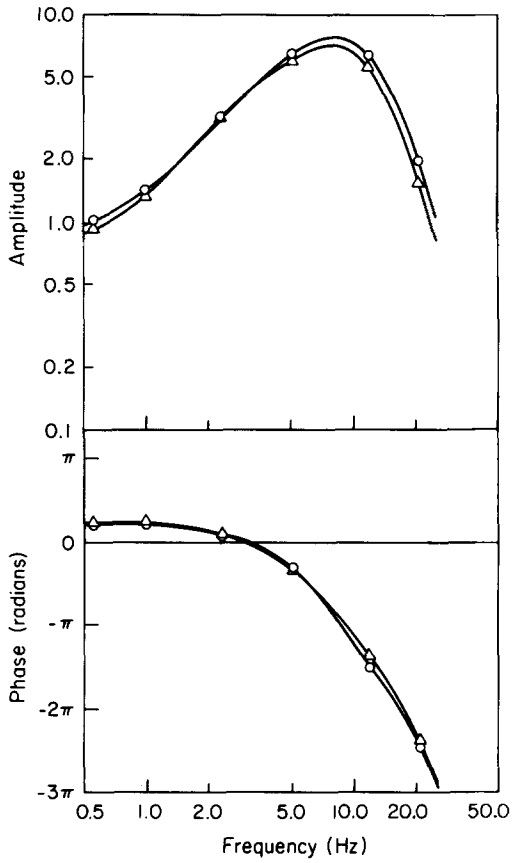

FIGURE A9. Comparison of light-to-impulse rate transfer functions: 76-μm diameter fiber-optic light pipe vs. oscilloscope-lens-fiber-optic taper optical system. The two transfer functions were obtained from the same test ommatidium: (○) light pipe, (△) fiber-optic taper. Mean impulse rates: light-pipe, 19.4 impulses/s; fiber-optic taper, 17.0 impulses/s. The figures show Bode plots (log amplitude vs. log frequency; phase vs. log frequency) of relative fractional modulation of output, taken as mean impulse density $r(t)$. Each curve is derived from pooled data from 12 presentations of the identical sum-of-sinusoids stimulus. (Frequencies were: 0.56, 1.00, 2.33, 5.15, 11.81, and 20.70 Hz.)

APPENDIX B

On the Choice of Output Variable for the Fourier Analysis of Impulse Train Data

The measurement of the harmonic content of various output variables has proved to be one of the most useful techniques for studying the dynamics of biological systems. When the output variable is a continuous function of time, such as muscle tension or an intracellular "slow potential," the application of

these Fourier methods is straightforward. On the other hand, when the output is a train of neural impulses, the information carried by the signal is presumably contained in the impulse occurrence times. In this case no function of continuous time is directly available for Fourier analysis. Several procedures for obtaining such a function have been proposed in the past (for example, French and Holden, 1971; Knight, 1972 *b*; Fohlmeister et al., 1977). We have recently adopted a procedure which determines the Fourier coefficients directly from the impulse occurrence times, without the intermediate calculation of a continuous time function. The method is equivalent to the use of post-stimulus-time histograms ("binning") with arbitrarily narrow bins. This procedure, its advantages, and its weaknesses, are discussed below.

In general, all calculations of Fourier coefficients may be interpreted as the result of a "least-squares" best-fitting procedure. Such a procedure determines those coefficients c_n that minimize a quadratic error estimator of the form:

$$\Delta = \int \{f(t) - \sum_n c_n f_n(t)\}^2 \mathrm{d}t, \tag{B1}$$

where the f_n are the functions with which we are attempting to approximate the data $f(t)$. (Here, for simplicity, we suppress the limits of integration and the corresponding division by the length of the interval of integration.) If the f_n are sines and cosines, the c_n are the usual Fourier coefficients, but other choices for f_n are equally suitable. In this context, the various procedures for Fourier analyzing impulse-train data amount to different explicit choices of the algorithm for obtaining $f(t)$, a function of a continuous variable, from the sequence of impulse occurrence times.

Once such a choice has been made, one may readily differentiate Eq. B1 with respect to the c_n; setting the partial derivatives $\partial\Delta/\partial c_m$ equal to zero yields a system of simultaneous equations for the c_n:

$$\int f(t) \cdot f_m(t) \mathrm{d}t = \sum_n c_n \cdot \int f_n(t) \cdot f_m(t) \mathrm{d}t, \qquad m = 1, 2 \cdots. \tag{B2}$$

If the f_n are orthogonal (as are the sines and cosines, if integrated over an integral number of periods), the correlation matrix $\int f_n(t) \cdot f_m(t) \mathrm{d}t$ reduces to $\delta_{n,m}$, and we retrieve the usual formula for the coefficients c_n.

The system of Eqs. B2 makes perfectly good sense if we allow $f(t)$ to be any suitably integrable function, even a sequence of Dirac delta-functions,

$$f(t) = \sum_k \delta(t - t_k),$$

where t_k is the time of occurrence of the k^{th} impulse. For this choice of f, we obtain the form:

$$\sum_k f_m(t_k) = \sum_n c_n \cdot \int f_n(t) \cdot f_m(t) \mathrm{d}t, \qquad m = 1, 2, \cdots. \tag{B3}$$

Unfortunately, such an f is not admissible in Eq. B1, because the δ-function is not square-integrable. Nonetheless, a careful limiting argument (in which one approximates the δ-function by a sequence of increasingly taller and narrower

rectangular pulses) demonstrates that Eq. B3 correctly calculates the spectral components associated with the impulse shape-independent structure of the impulse train. Under the assumption that only the impulse occurrence times convey information of interest, this is no limitation. We will refer to the set of Fourier components c_n obtained from Eq. B3 as the "delta-function spectrum."

This calculation of the delta-function spectrum has several computational advantages. First the correlation matrix $\int f_n(t) f_m(t) dt$ can be calculated in advance; it depends only on the functions f_n and the interval over which data are collected. Second, the calculation is linear in the data; thus, if data from several episodes with identical stimuli are to be pooled, one may simply add together the function values $f_m(t_k)$ from all episodes. Third, the algorithm is well suited to on-line data acquisition: if tables of the functions f_n are stored in memory, a pointer incremented in real time can provide rapid access to the function value $f_n(t_k)$, so that whenever an impulse occurs, the current function value is immediately available for addition to a running total. The same function table may even serve to provide a list of successive stimulus values. Such a scheme has recently been implemented with a microprocessor-driven device in our laboratory (Milkman et al., 1978).

Because the delta function spectrum calculation is linear, as described above, it follows immediately that, as the number of pooled impulse trains grows large, the Eqs. B3 approach the continuous system (Eqs. B2), if we make the choice $f(t) = r(t)$, where $r(t)$ is the mean impulse density function as defined in Eq. 22, above.

Another important feature of the formulation above is the provision for nonorthogonal functions f_n. In general, a "ramp" function $f_n(t) = t - t_o$ will not be orthogonal to both a sine and cosine function over any time interval. Similarly, sinusoids of incommensurate periods fail to be orthogonal, as do commensurate sinsuoids except over carefully selected time intervals. The flexibility of the system (Eqs. B3) in dealing with such functions greatly facilitates the selection of episode lengths.

The various alternative choices for the function $f(t)$ generally fall into two classes. "Binning" methods are particularly simple to apply. They divide the episode into short successive equal time periods ("bins"), and assign to each such period the number of impulses which occur within it. "Instantaneous rate" methods, which are often useful for impulse trains with few impulses, assign function values equal to the reciprocals of the time intervals between impulses. It is also possible to combine these approaches. For impulse trains varying about a mean carrier rate, all of these functions convey the same information and are simply related by transfer functions, such as that calculated in Eqs. 25–28. Nonetheless, the delta-function procedure outline above has several relative advantages in experimental situations.

First, the delta-function spectrum is highly insensitive to discrimination errors, which may result in erroneously short intervals between impulses. These experimental artifacts greatly distort calculations based on reciprocal intervals, but scarcely perturb the running sums from which the delta-function spectrum is calculated. Indeed, any number of spurious impulses uncorrelated with the

periodic stimulus have no systematic effect on the computed spectrum. Second, unlike the results of binning procedures, the delta-function spectrum contains no nulls due to the interaction of a modulation frequency component with the bin width (a parameter which is entirely external to the system under study). Finally, both binning and reciprocal interval methods suffer from phase errors, because the procedures which produce the function $f(t)$ somewhat distort the time at which an impulse is reflected in the spectral estimation; in contrast, the delta-function procedure accurately reflects each impulse at the time when it actually occurs.

In summary, the delta-function spectrum, as determined by the system of Eqs. B3, provides an excellent and easily computed characterization of the harmonic content of impulse train data. The procedure is free from many of the artifacts which affect other methods when applied to laboratory data, and it imposes no arbitrary structure of its own on the data.

We thank James Gordon for his assistance with the photographs which appear in Appendix A. This work was supported, in part, by National Institutes of Health grants EY 188, EY 1428, EY 1472, and GM 1789.

Received for publication 5 January 1978.

REFERENCES

ADOLPH, A. R. 1971. Recording of optic nerve spikes underwater from freely-moving horseshoe crab. *Vision Res.* **11**:979–983.

ADOLPH, A. R. 1973. Thermal sensitivity of lateral inhibition in *Limulus* eye. *J. Gen. Phsyiol.* **62**:392–406.

BARLOW, R. B. 1967. Inhibitory fields in the *Limulus* lateral eye. Thesis, The Rockefeller University, New York.

BARLOW, R. B., and G. D. LANGE. 1974. A nonlinearity in the inhibitory interactions in the lateral eye of *Limulus*. *J. Gen. Physiol.* **63**:579–589.

BIEDERMAN-THORSON, M., and J. THORSON. 1971. Dynamics of excitation and inhibition in the light-adapted *Limulus* eye *in situ*. *J. Gen. Physiol.* **58**:1–19.

BRODIE, S. E. 1978. Temperature dependence of the dynamic response of the *Limulus* retina. *Vision Res.* In press.

BRODIE, S. E., B. W. KNIGHT, and F. RATLIFF. 1978. The spatiotemporal transfer function of the *Limulus* lateral eye. *J. Gen. Physiol.* **72**:000–000.

CORNING, W. C., D. A. FEINSTEIN, and J. R. HAIGHT. 1965. Arthropod preparation for behavioral, electrophysiological, and biochemical studies. *Science (Wash. D.C.)*. **148**:394–395.

FOHLMEISTER, J. F., R. E. POPPELE, and R. L. PURPLE. 1977. Repetitive firing: a quantitative study of feedback in model encoders. *J. Gen. Physiol.* **69**:815–848.

FRENCH, A. S., and A. V. HOLDEN. 1971. Alias-free sampling of neuronal spike trains. *Kybernetik.* **8**:165–171.

GAUSS, C. F. 1828. Disquitiones generales circa superficies curvas. *Commentat. Soc. R. Sci. Gott. Recent.* **6**:99–146.

HARTLINE, H. K., and C. H. GRAHAM. 1932. Nerve impulses from single receptors in the eye. *J. Cell. Comp. Physiol.* **1**:227–295.

HARTLINE, H. K., and F. RATLIFF. 1957. Inhibitory interaction of receptor units in the eye of *Limulus*. *J. Gen. Physiol.* **40**:357–376.

HARTLINE, H. K., and F. RATLIFF. 1972. Inhibitory interaction in the retina of Limulus. *In* Handbook of Sensory Physiology, Vol. VII/2, Physiology of Photoreceptor Organs, M. G. F. Fuortes, editor. Springer-Verlag, Berlin. 381–447.

KAPANY, N. S. 1967. Fiber Optics: Principles and Applications. Academic Press, Inc. New York. 429 pp.

KAPLAN, E., and R. B. BARLOW, JR. 1975. Properties of visual cells in the lateral eye of *Limulus in situ*. *J. Gen. Physiol.* **66**:303–326.

KIRSCHFELD, K., and W. REICHARDT. 1964. Die Verarbeitung stationärer optischer Nachrichten im Komplexauge von Limulus. Ommatidien-Sehfeld und räumliche Verteilung der Inhibition. *Kybernetik.* **2**:43–61.

KNIGHT, B. W., J. TOYODA, and F. A. DODGE. 1970. A quantitative description of the dynamics of excitation and inhibition in the eye of Limulus. *J. Gen. Physiol.* **56**:421–437.

KNIGHT, B. W. 1972 *a*. Dynamics of encoding in a population of neurons. *J. Gen. Physiol.* **59**:734–766.

KNIGHT, B. W. 1972 *b*. The relationship between the firing rate of a single neuron and the level of activity in a population of neurons. *J. Gen. Physiol.* **59**:767–778.

MACNICHOL, E. F., and J. A. H. JACOBS. 1955. Electronic device for measuring reciprocal time intervals. *Rev. Sci. Instrum.* **26**:1176–1180.

MILKMAN, N., R. SHAPLEY, and G. SCHICK. 1978. A microcomputer based visual stimulator. *Behav. Res. Methods Instrum.* In press.

RATLIFF, F. 1965. Mach Bands: Quantitative Studies on Neural Networks in the Retina. Holden-Day, Inc., San Francisco. 365 pp.

RATLIFF, F., editor. 1974. Studies on Excitation and Inhibition in the Retina. The Rockefeller University Press, New York. 668 pp.

RATLIFF, F., B. W. KNIGHT, and N. GRAHAM. 1969. On tuning and amplification by lateral inhibition. *Proc. Natl. Acad. Sci., U. S. A.* **62**:733–740.

RATLIFF, F., B. W. KNIGHT, J. TOYODA, and H. K. HARTLINE. 1967. Enhancement of flicker by lateral inhibition. *Science. (Wash. D. C.).* **158**:392–393.

RATLIFF, F., and L. SIROVICH. 1978. Equivalence classes of visual stimuli. *Vision Res.* In press.

SHAPLEY, R., and M. ROSSETTO. 1976. An electronic visual stimulator. *Behav. Res. Methods Instrum.* **8**:15–20.

STEVENS, S. S. 1975. Psychophysics. John Wiley and Sons, New York. 329 pp.

VICTOR, J. D., R. M. SHAPLEY, and B. W. KNIGHT. 1977. Nonlinear analysis of cat retinal ganglion cells in the frequency domain. *Proc. Natl. Acad. Sci., U. S. A.* **74**:3068–3072.